

# We are IntechOpen, the world's leading publisher of Open Access books Built by scientists, for scientists

6,900

Open access books available

185,000

International authors and editors

200M

Downloads

Our authors are among the

154

Countries delivered to

TOP 1%

most cited scientists

12.2%

Contributors from top 500 universities



WEB OF SCIENCE™

Selection of our books indexed in the Book Citation Index  
in Web of Science™ Core Collection (BKCI)

Interested in publishing with us?  
Contact [book.department@intechopen.com](mailto:book.department@intechopen.com)

Numbers displayed above are based on latest data collected.  
For more information visit [www.intechopen.com](http://www.intechopen.com)



# Biomaterials and Sol-Gel Process: A Methodology for the Preparation of Functional Materials

Eduardo J. Nassar et al\*

*Universidade de Franca, Franca, Sao Paulo,  
Brazil*

## 1. Introduction

There are many kinds of materials with different applications. In this context, biomaterials stand out because of their ability to remain in contact with tissues of the human body. Biomaterials comprise an exciting field that has been significantly and steadily developed over the last fifty years and encompasses aspects of medicine, biology, chemistry, and materials science. Biomaterials have been used for several applications, such as joint replacements, bone plates, bone cement, artificial ligaments and tendons, dental implants for tooth fixation, blood vessel prostheses, heart valves, artificial tissue, contact lenses, and breast implants [1]. In the future, biomaterials are expected to enhance the regeneration of natural tissues, thereby promoting the restoration of structural, functional, metabolic and biochemical behaviour as well as biomechanical performance [2]. The design of novel, inexpensive, biocompatible materials is crucial to the improvement of the living conditions and welfare of the population in view of the increasing number of people who need implants [3]. In this sense, it is necessary that the processes employed for biomaterials production are affordable, fast, and simple to carry out. Several methodologies have been utilized for the preparation of new bioactive, biocompatible materials with osteoconductivity, and osteoinductivity [4 - 13]. New biomaterials have been introduced since 1971. One example is Bioglass 45S5, which is able to bind to the bone through formation of a hydroxyapatite surface layer [14]. The sol-gel processes are now used to produce bioactive coatings, powders, and substrates that offer molecular control over the incorporation and biological behavior of proteins and cells and can be applied as implants and sensors [15 - 17]. In the literature there are several works on the use of the sol-gel process for production of biomaterials such as nanobioactive glass [18], porous bioactive glass [19], and bioactive glass [20 - 22], among others.

Hybrid inorganic-organic nanocomposites first appeared about 20 years ago. The sol-gel process was the technique whose conditions proved suitable for preparation of these materials and which provided nanoscale combinations of inorganic and organic composites

---

\* Katia J. Ciuffi, Paulo S. Calefi, Lucas A. Rocha, Emerson H. De Faria, Marcio L. A. e Silva, Priscilla P. Luz, Lucimara C. Bandeira, Alexandre Cestari, Cristianine N. Fernandes  
*Universidade de Franca, Franca, Sao Paulo, Brazil*

[23]. Natural bone is an inorganic-organic composite consisting mainly of nanohydroxyapatite and collagen fibers. Hybrid materials obtained by the sol-gel route combine the advantages of both organic and inorganic properties. Several kinds of organofunctional alkoxysilanes precursors have been studied for the production of silica nanoparticles. The sol-gel offers advantages such as the possibility of obtaining homogeneous hybrid materials under low temperature, thereby allowing for the incorporation of a variety of compounds [23 - 29].

The sol-gel process is based on the hydrolysis and condensation of metal or silicon alkoxides and is used to obtain a variety of high-purity inorganic oxides or hybrid inorganic-organic materials that are simple to prepare [30]. This process can be employed for the synthesis of functionalized silica with controlled particle size and shape [31 - 38].

Apart from the several applications mentioned in the first paragraph of this chapter, more recently, biomaterials have been utilized as drug delivery systems (DDSs). In this sense, polymers and biodegradable polymers emerge as potential materials, since they promote temporal and targeted drug release. Indeed, biomaterials have had an enormous impact on human health care. Applications include medical devices, diagnosis, sensors, tissue engineering, besides the aforementioned DDSs [39]. In the latter field, an ideal drug deliverer should be able to lead a biologically active molecule at the desired rate and for the desired duration to the desired target, so as to maintain the drug level in the body at optimum therapeutic concentrations with minimum fluctuation [1, 40]. The use of DDSs overcomes the problems related to conventional administration routes, such as oral and intravenous administration.

Several biomaterials have been applied as DDSs. This is because they are biocompatible and/or biodegradable, which allows for consecutive administrations. Hydroxyapatite-based materials, natural and synthetic polymers, silica, clays and other layered double hydroxides, and lipids are some examples of biomaterials that have been employed for the delivery of active molecules through the body. Liposomes, solid lipid nanoparticles, polymeric nano and microparticles, micelles, dendrimers, metallic nanoparticles, and nanoemulsion are currently utilized as DDSs.

Special attention has been given to DDSs comprised of biodegradable polymers and silica. In polymeric DDSs, the drugs are incorporated into a polymer matrix. Since biodegradable polymers are degraded to non-toxic substances, they do not have to be removed after implantation. So they have become attractive candidates for DDS applications. The rate of drug release from polymeric matrices depends on several parameters such as the nature of the polymer matrix, matrix geometry, drug properties, initial drug loading, and drug-matrix interaction. Moreover, the drugs can be effectively released by bioerosion of the matrices. [40]. Thus, both natural, frequently polysaccharides, and synthetic biodegradable polymers, usually aliphatic polyesters such as PLA, PGA, and their copolymer (PLGA), are the most extensively investigated biodegradable materials for drug delivery applications [1]. Inorganic materials, like silica, can offer the necessary properties for a nanoparticle to be applied as DDS, especially nontoxicity, biocompatibility, high stability, and a hydrophilic and porous structure. The drug release rate from the silica structures could be controlled by adjusting particle size and porous structure [41 - 45].

The sol-gel technology is also employed in the preparation of inorganic ceramic and glass materials. This technique was first used in the mid 1800s, when Ebelman and Graham carried out studies on silica gels [46]. Initially, the sol-gel process was utilized in the preparation of silicate from tetraethylorthosilicate (TEOS,  $\text{Si}(\text{OC}_2\text{H}_5)_4$ ), which is mixed with

water and a mutual solvent, to form a homogeneous solution. Recently, new reagents have appeared, so novel inorganic oxides and hybrid organic-inorganic materials can be synthesized using this methodology. Another process known as non-hydrolytic sol-gel has been developed by Acosta et al [47], who used the condensation reaction between a metallic or semi-metallic halide (M-X) and a metallic or semi-metallic alkoxide (M'-OR) to obtain an oxide (M-O-M'). The hydrolytic and non-hydrolytic sol-gel processes as well as their mechanisms are well discussed in the literature [46, 48, 30]. The sol-gel route is well-known for its simplicity and high rates. It is the most commonly employed technique for the synthesis of nanoparticles, and it involves the simultaneous hydrolysis and condensation reaction of the alkoxide or salt. The obtained materials have several particular features. The importance and advantages of nanoparticles have been scientifically demonstrated, and these particles have several industrial applications; e.g., in catalysis, pigments, biomaterials, phosphors, photonic devices, pharmaceuticals, and among others [36, 49 - 54]. In this chapter, we propose a brief review on materials prepared by the hydrolytic and non-hydrolytic sol-gel methodologies and their possible bioapplications.

## 2. Results and discussion

In the next topics, 2.1 and 2.2, the results and discussion about all the research developed in our laboratory using hydrolytic and non-hydrolytic methodologies in the synthesis of materials for bio applications such as glass ionomers, bioactive materials, coating on scaffolds obtained by rapid prototyping (RP), and materials for drug delivery are shown.

### 2.1 Preparation of biomaterials by the hydrolytic sol-gel process

In this topic the materials prepared by the hydrolytic sol-gel methodology and their characterization are described. We aimed to obtain materials whose properties would enable their application as biomaterials.

In a first work, materials containing Ca-P-Si were prepared by the sol-gel route by mixing TEOS, calcium alkoxide, and phosphoric acid [55]. The resulting materials were immersed in Simulated Body Fluid (SBF) [56], pH = 7.40, for 12 days. The sample was characterized before and after contact with SBF.

Transmission electron microscopy (TEM) can provide structural information about materials, such as particle shape, size, and crystallinity. Figures 1a, b, c, and d show TEM images of the Ca-P-Si matrix obtained by the sol-gel methodology before and after immersion in SBF.

The TEM images in Figure 1a reveal the formation of small particles with an average size of 20 nm. Electron diffraction gives evidence of an amorphous phase. The bright and dark fields in Figures 1b and c demonstrate that the materials contain crystalline and amorphous phases. Figure 1d displays the electron diffraction of the crystalline phase. The electron diffraction pattern shows planar distances of 2.86 Å and 1.88 Å, which, according to Bragg's law, indicates that these distances correspond to  $2\theta = 31.2^\circ$  (211) and  $48.6^\circ$  (320). This peak can be ascribed to hydroxyapatite (JCPDS - 9-0432) [57]. The EDS spectra of the amorphous phase reveal large quantities of Si and O, indicating the presence of amorphous silicate. The crystalline phase, whose composition contained Ca and P, has been ascribed to hydroxyapatite crystallization.

In another work, samples with different Ca/P molar ratios were prepared by the sol-gel methodology, by mixing TEOS, calcium ethoxide, and phosphoric acid. The samples were analyzed before and after contact with SBF [50].

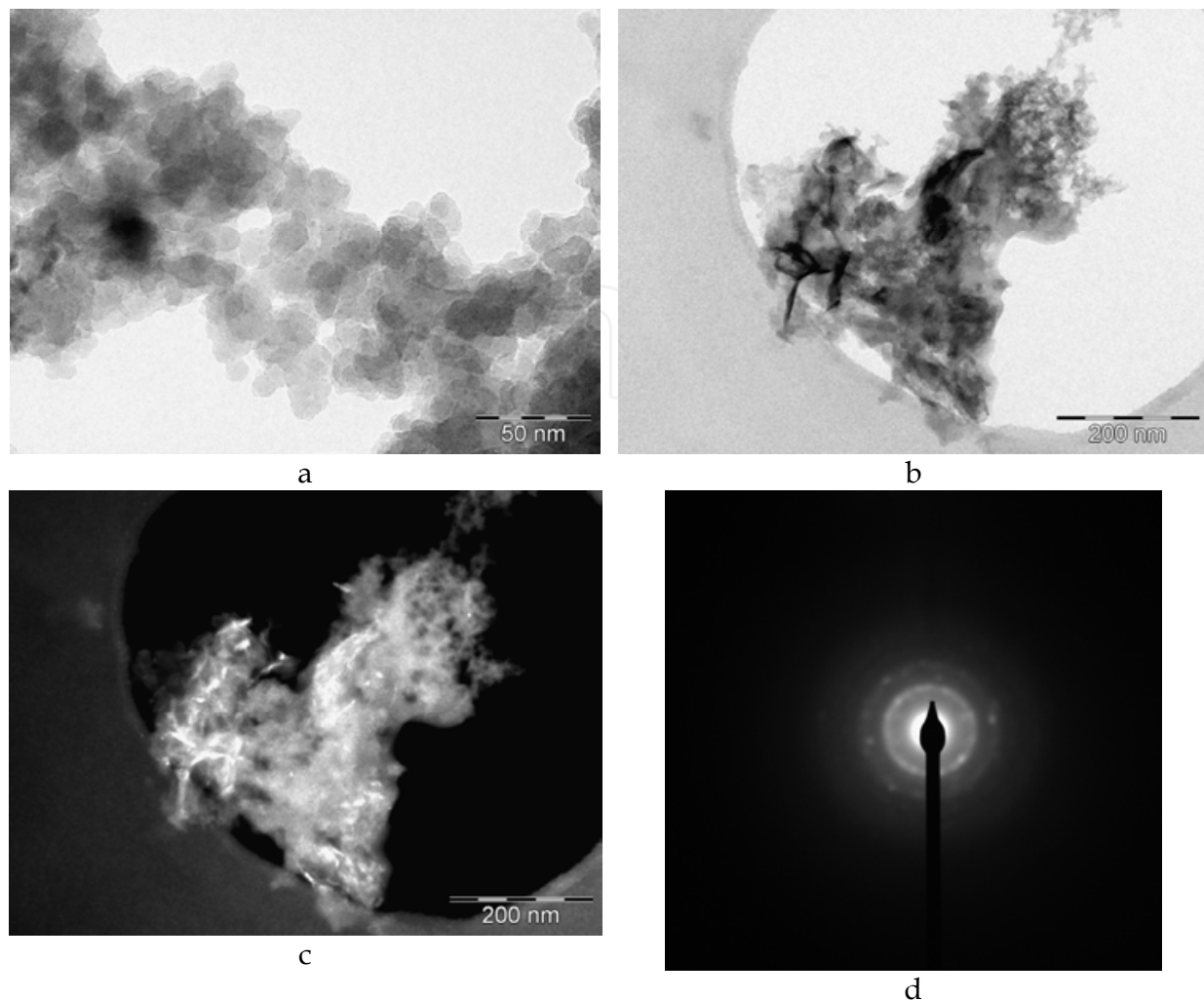


Fig. 1. TEM images of the Ca-P-Si matrix before (a) and after (b) immersion in SBF, bright (b) and dark field (c), and electron diffraction (d) of the sample's crystalline phase after immersion in SBF.

Figures 2 and 3 depict the X-ray diffraction patterns for the samples prepared with different Ca/P molar ratios, before and after contact with the SBF solution, respectively.

The three starting powders present crystalline and amorphous phases, with well-defined diffraction peaks. The crystalline phase displays peaks at  $2\theta = 26.5, 32.5, 33.0, 49.2,$  and  $53.1$ , which can be ascribed to hydroxyapatite (HA), whereas the peaks corresponding to calcium triphosphate (TCP- $\beta$ ) appear at  $2\theta = 26.5, 30.2,$  and  $53.1$ . [58]. Several other peaks due to other phosphate silicates, such as  $\text{Ca}_5(\text{PO}_4)_2\text{SiO}_4$  and  $(\text{Ca}_2(\text{SiO}_4))_6(\text{Ca}_3(\text{PO}_4)_2)$ , can also be observed.

The high percentages of phosphate ions (40%) in the present samples were crucial to the precipitation of crystalline phosphate nanoparticles in the silica matrix. However, according to literature reports, the double  $\text{P}=\text{O}$  bond favors phosphate phase formation in the silica network, thus increasing the tendency toward crystallization [59]. The peak broadening of the XRD reflection can be used to estimate crystallite size in a direction perpendicular to the crystallographic plane, using the Scherrer equation [60]. On the basis of the XRD data, the average crystallite size was calculated as being approximately 2 nm, which indicates the formation of calcium phosphate nanoparticles.



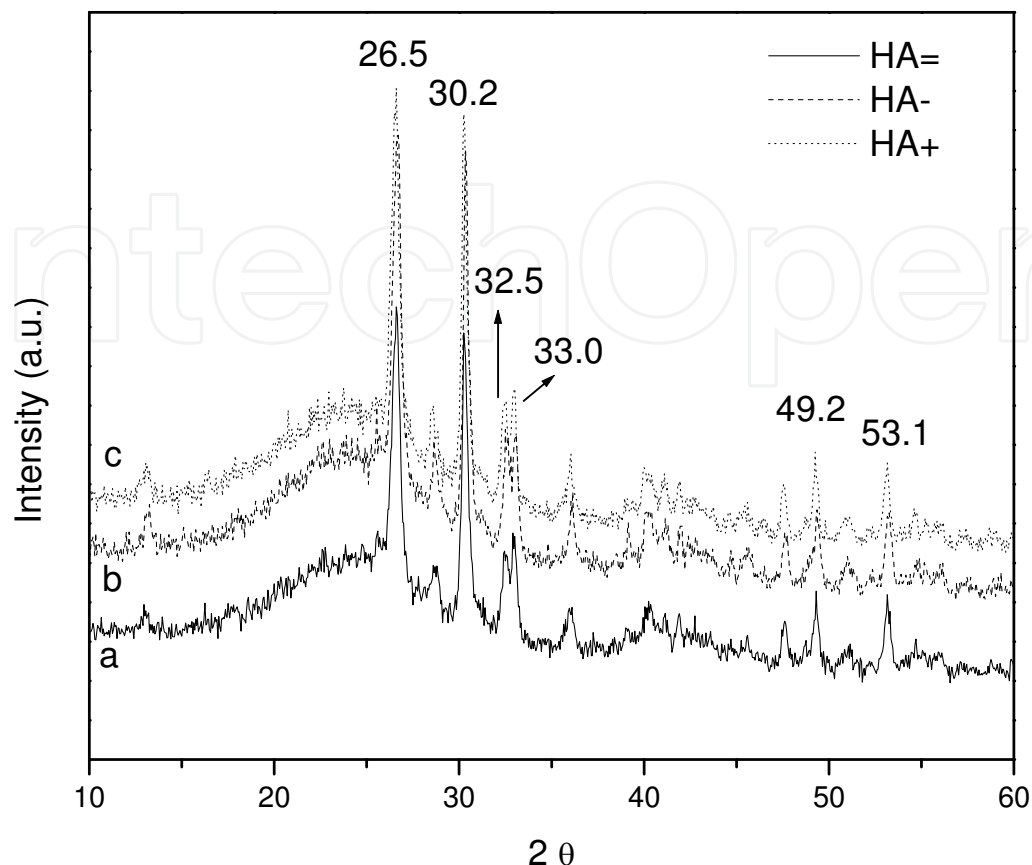


Fig. 2. X-ray diffraction of the samples (a) = HA, (b) HA-, and (c) HA+ before contact with SBF.

The technology based on RP is a processes employed for assemblage of materials in the powder, filament, liquid, or slide form, which in turn are stacked in successive thin layers until a three-dimensional structure is achieved. The process begins by designing a mold for the scaffold using computer-aided design (CAD) software. The mold can possess a branching network of shafts that will define the microchannels in the scaffold [61 - 65]. The layer-by-layer building approach allows for the preparation of highly complex structures that cannot be obtained by technologies based on material subtraction, which is the most frequently employed procedure nowadays. RP has several important applications in a number of areas, including aircrafts, automobiles, telecommunications, and medicine [66 - 68].

In our following works 3D piece prepared by RP on ABS and polyamide (nylon) was used, and the properties of this piece were modified by the sol-gel methodology. To this end, the sols were prepared by stirring TEOS and calcium alkoxide in ethanol. Two sols were synthesized, namely one containing phosphate ions (Si-Ca-P) and another without phosphate (Si-Ca) [69]. The sols were deposited onto ABS by using the dip-coating, as described in the literature [70, 71]. This technique consists in immersing a substrate directly into the prepared sols. The crystallization of phosphates was accomplished by immersing the samples into SBF for 15 days. The SBF treatment was performed in the static condition. The samples were then dried at 50°C and characterized.

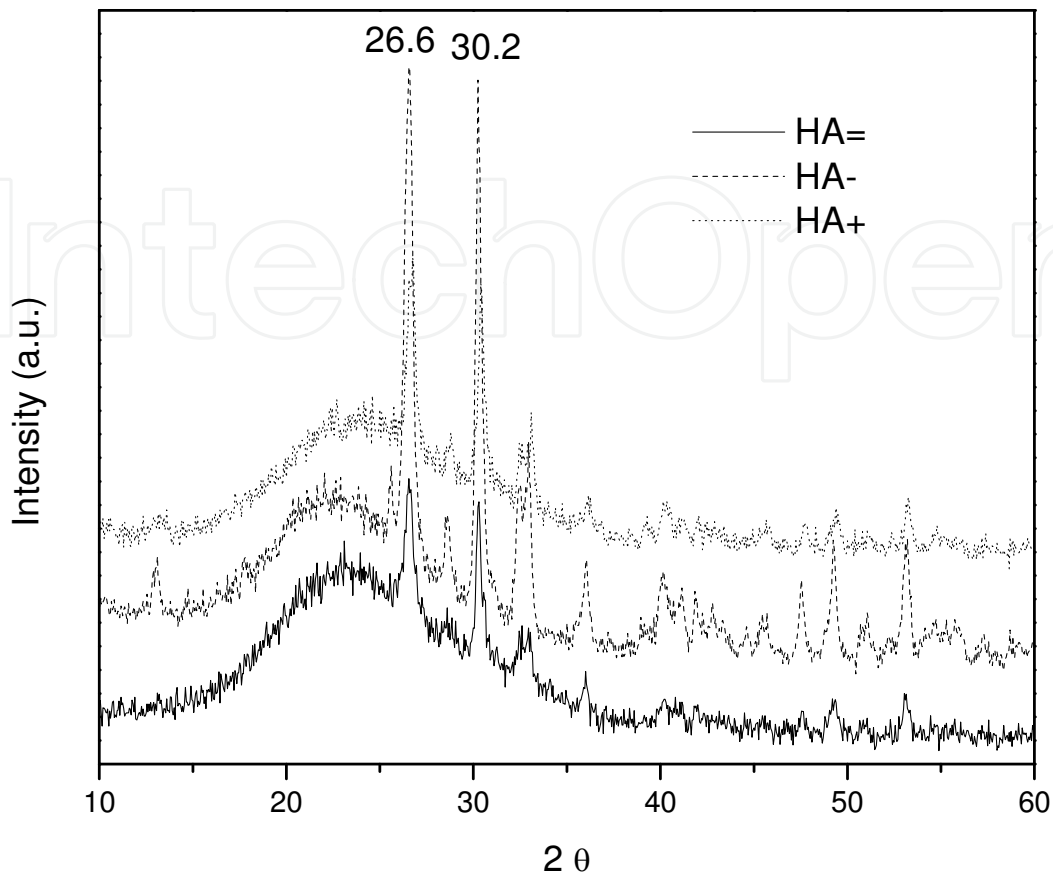


Fig. 3. X-ray diffraction of the samples (a) = HA, (b) HA-, and (c) HA+ after contact with SBF.

Figure 4 displays the XRD patterns obtained for the ABS substrate and for the AcP and AsP samples.

XRD analysis of the ABS substrate and of the samples coated by sol-gel revealed the presence of broad peaks between 10 and 30°, characteristic of amorphous materials. Figures 5 and 6 illustrate the XRD patterns of the samples AcP and AsP before and after contact with SBF, respectively.

After contact with SBF, the XRD patterns of the samples AcP and AsP clearly displayed peaks, which is evidence of initial crystallization. Peaks at  $2\theta = 10.6, 21.6, 31.6,$  and  $45.2$  were detected for the AcP sample after it was placed in SBF for 15 days, whereas the XRD pattern of the sample AsP displayed two peaks only, namely at  $2\theta = 31.6$  and  $44.9$ . The latter peaks correspond to a mixture of calcium phosphate silicates (JCPDS 21-0157; 11-0676). This observation is very important since it shows that the coating interacts with SBF to form a calcium phosphate, which is the main component of hydroxyapatite. Infrared spectroscopy of the ABS substrate presented peaks at  $1077$  and  $465\text{ cm}^{-1}$ , ascribed to the Si-O-Si vibration mode. These peaks were also verified in the spectrum of the sample AcP after contact with SBF, indicating that the silicate coating is still present on the ABS substrate. New peaks appeared at  $3360$  and  $1653\text{ cm}^{-1}$ , related to water vibrations, and at  $610$  and  $550\text{ cm}^{-1}$ , ascribed to the P-O vibration [72], thereby corroborating the observations from the X-ray

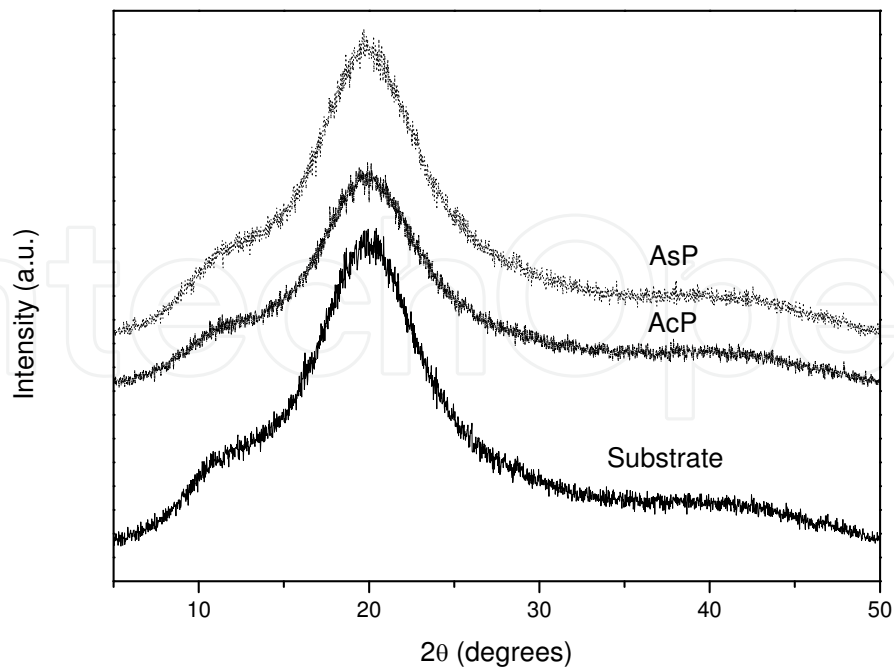


Fig. 4. XRD analysis of the ABS substrate and the ABS-coated samples AcP and AsP.

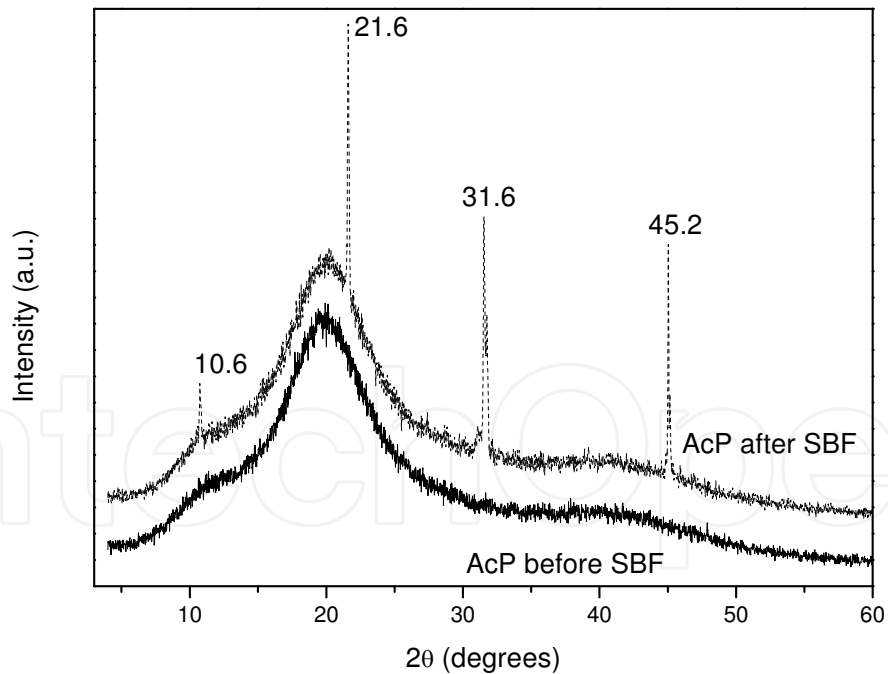


Fig. 5. XRD of the sample AcP before and after contact with SBF.

analysis and evidencing formation of the calcium phosphate silicate. The FTIR-ATR spectrum recorded for the sample AsP after contact with SBF displayed peaks characteristic of crystalline phosphate at 600 and 560  $\text{cm}^{-1}$ , and carbonate hydroxyapatite, at 1451, 1408, and 874  $\text{cm}^{-1}$  [72]. This suggests that these materials can be used for bioapplications.



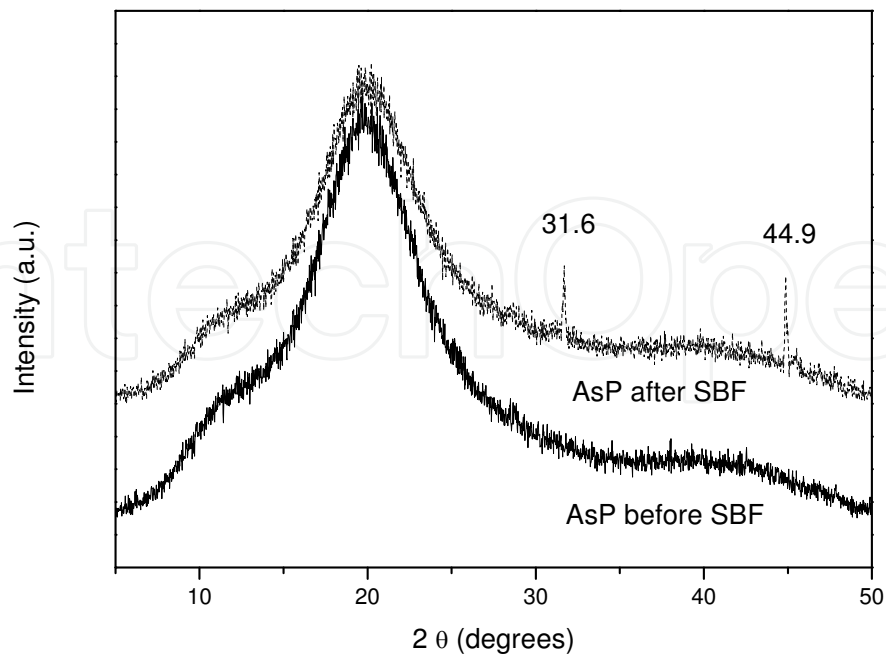


Fig. 6. XRD of the sample AsP before and after contact with SBF.

Changes in the properties of macroporous (pore size = 500μm) samples of the polymers polyamide 12 (nylon) and ABS, obtained by RP, were investigated herein. Sols containing silicon and calcium alkoxide, with or without phosphate anions, were deposited onto the polymers by the dip-coating technique [73]. The goal of this work was to coat the organic polymer materials with macroporous compounds and verify whether the resulting materials can be used as biomaterials. If the homogeneous composition of a coating can transform an organic polymer into a biocompatible material, then the latter can be applied in bone implant. RP promotes the building of pieces with different and complex forms. Figure 7 is a representation of the substrates based on the organic polymers polyamide 12 (nylon) and ABS prepared by RP, with a pore size of 500μm.

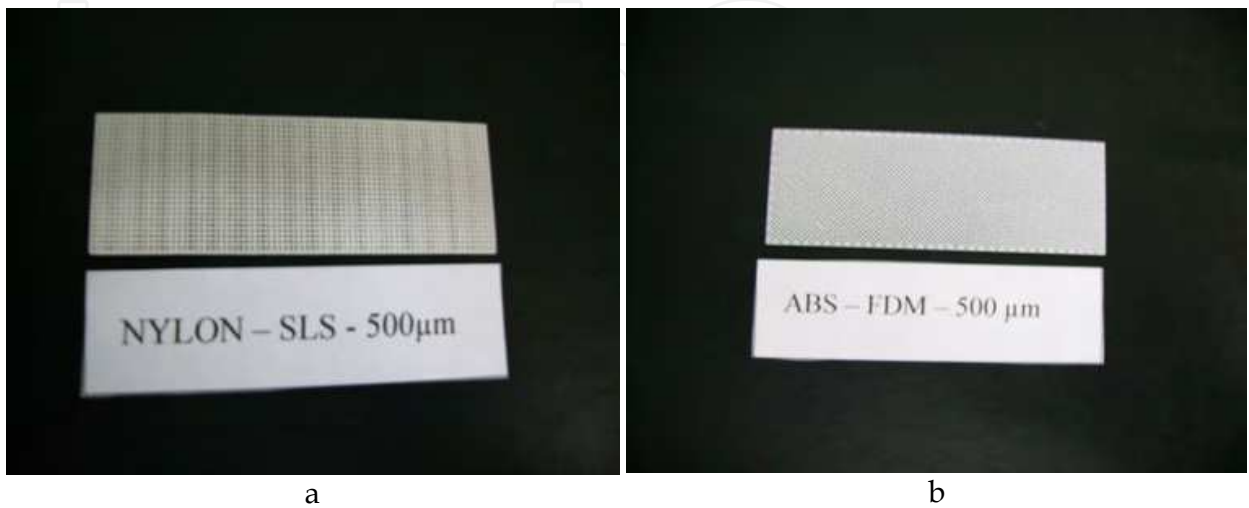


Fig. 7. Porous materials prepared by RP: (a) polyamide 12 and (b) ABS.

The SEM micrographs show that the polymers exhibit different surfaces. Polyamide 12 is rough, whereas ABS is smooth. Surface features can affect adherence of the coating to the polymer. Figure 8a, b, c, and d depict the SEM micrographs of polyamide 12 and ABS after coating with Si-Ca-P and Si-Ca, respectively.

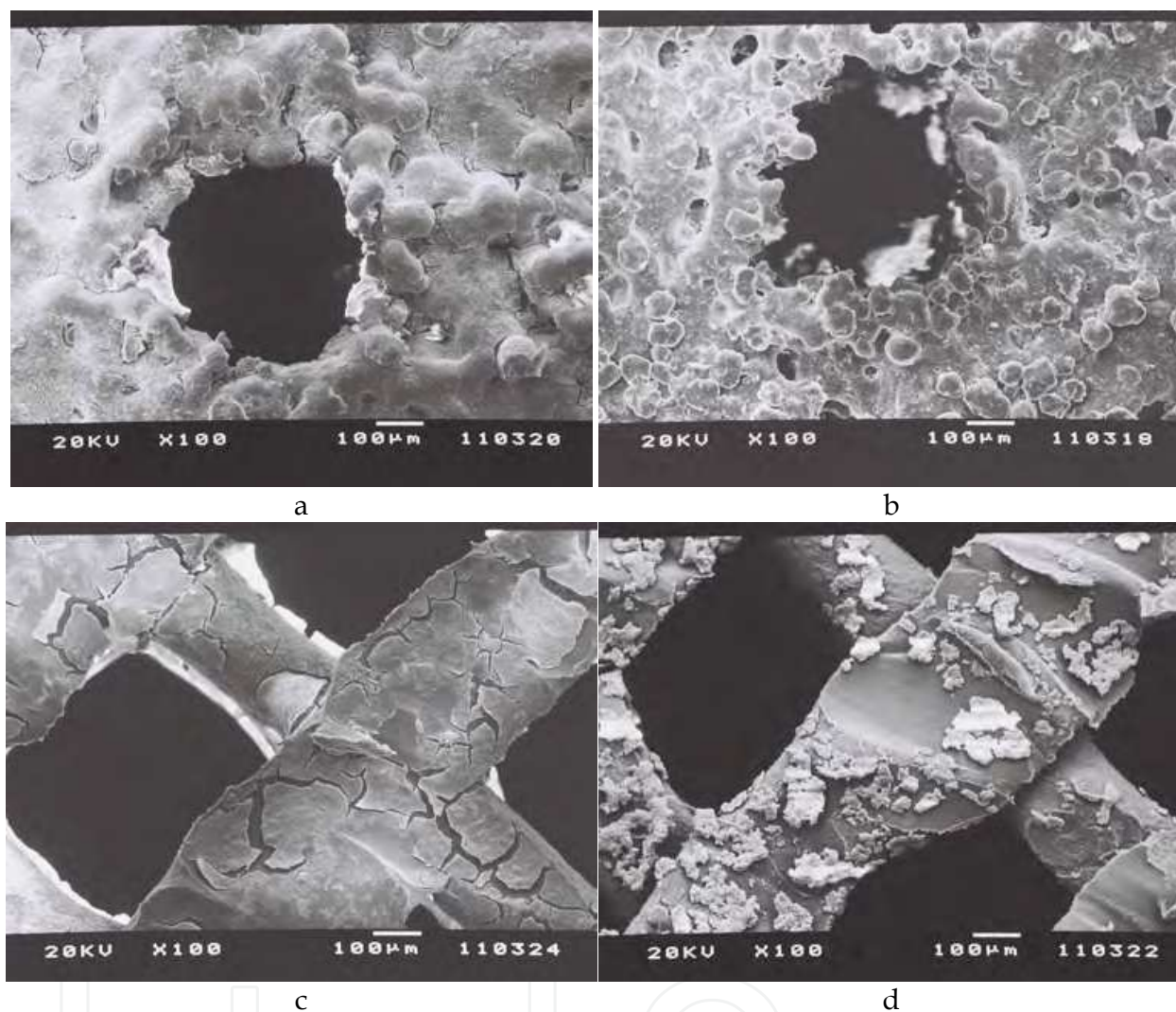


Fig. 8. SEM micrographs of the coated polymers: (a) polyamide 12 + Si-Ca-P, (b) polyamide 12 + Si-Ca, (c) ABS + Si-Ca-P, and (d) ABS + Si-Ca.

SEM furnishes information about the homogeneity, shape, size, and adherence of materials, which aids explanation about the change in the properties of the coated polyamide 12 and ABS. The polyamide 12 polymer has an initial pore size of 500  $\mu\text{m}$ , which is reduced to 300  $\mu\text{m}$  after coating and RP. This leads to the conclusion that the coating has a thickness of 200  $\mu\text{m}$ . The coating prepared by combination of the sol-gel methodology with the dip-coating technique produces films with sizes in the nanometer range [74, 75]. In the present case, the compositions of both the sol and the polymer promote an increase in thickness. The thickness of the coating in polyamide 12 and ABS polymers influences the decomposition temperature, and thicker coatings lead to higher decomposition temperatures. This observation is corroborated by the SEM technique. The same coating was prepared on a 3D piece, represented in Figure 9.

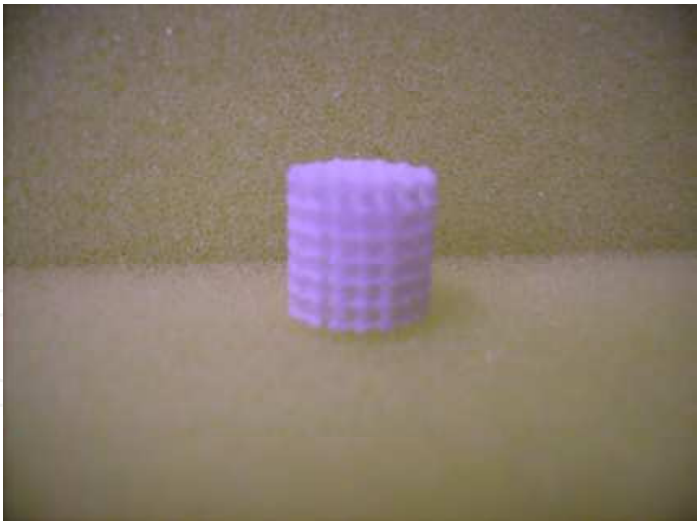


Fig. 9. 3D piece of the polyamide structured by RP.

Bioactivity tests in SBF and fibroblast cell cultures were performed. There was growth of differentiated cells in the fibroblast culture for both functionalized polyamide and ABS. Figures 10 a, b, c, and d correspond to the results obtained with polyamide 12 without and with coating and ABS without and with coating after 4 days, respectively. It was possible to observe that the cells were not affected by the coating, showing that the materials present potential future applications for use in biomaterials.

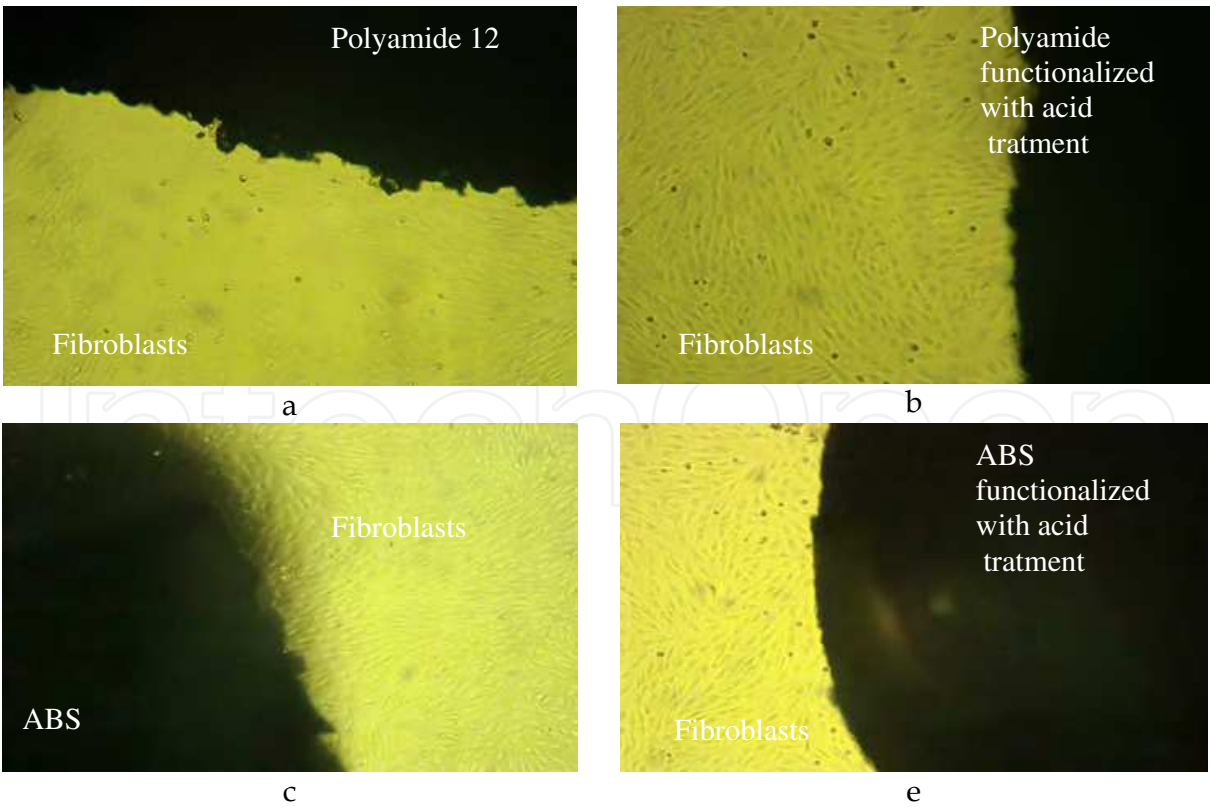


Fig. 10. Polyamide and ABS without and with coating after immersion into fibroblast cell culture for four days.



Formation of calcium phosphate on the polyamide substrate obtained by RP can be achieved by means of the sol-gel process. So a sol containing tetraethylorthosilicate, calcium alkoxide, phosphoric acid, and alginate was prepared. Figures 11 a and b depict the micrograph of the resulting substrate.

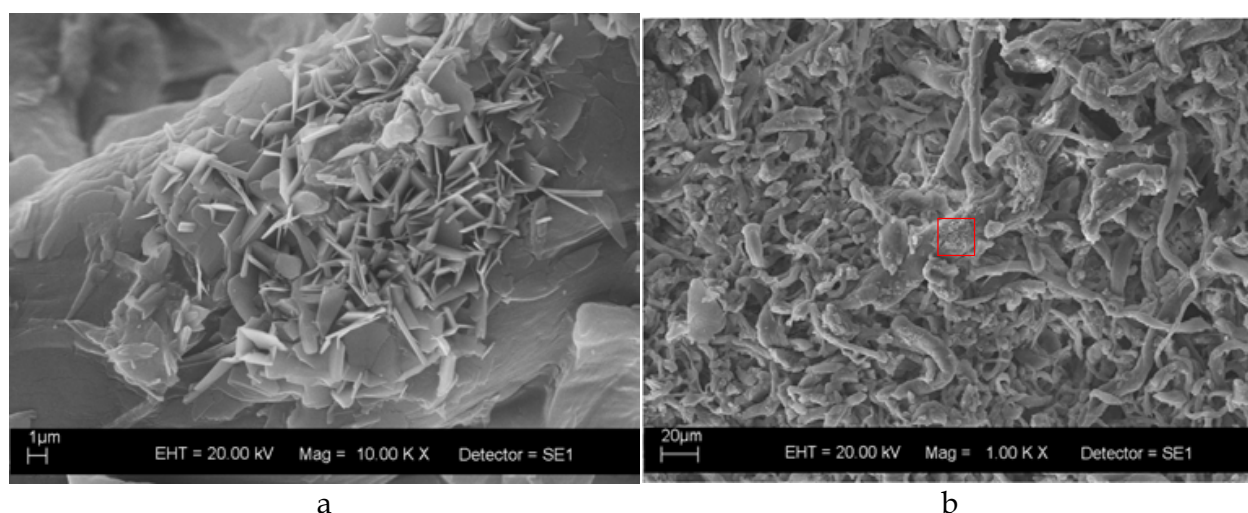


Fig. 11. Polyamide substrate functionalized with Si-Ca-P-alginate.

From Figure 11a it can be seen that calcium phosphate was formed on the alginate fibers. In Figure 11b, the alginate fibers and the red square corresponding to the calcium phosphate crystals can be observed. The EDS spectrum confirms the presence of the Si-Ca-P elements in the crystals. This material is a candidate for use in bone implant.

Silica nanospheres were prepared in order to test their use as DDS. In addition, a factorial design was developed, so that the influence of hydrolytic base-catalyzed sol-gel parameters and surfactant (Tween 80 or Pluronic F68) concentration over the nanoparticles morphology could be analyzed.

SEM characterization showed that the two surfactants employed herein provided very

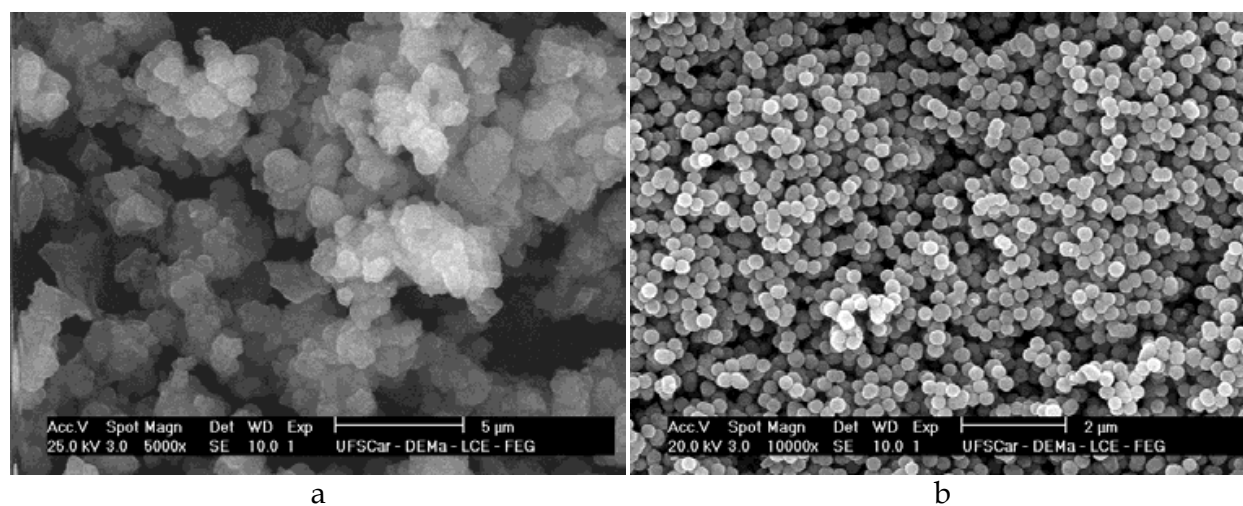


Fig. 12. SEM images of the particles prepared by the hydrolytic sol-gel using (a) Pluronic F68 and (b) Tween 80 as surfactants.

different results. In general, the particles prepared using Tween 80 were more spherically shaped compared to those prepared with Pluronic F68. Figure 12 displays two examples of particles obtained from the factorial design, prepared under the same conditions, but with different surfactants.

The spherical and nanometric particles presented in Figure 12b meet the requirements of the morphology desired for a DDS. This morphology allows for different administration routes, including the intravenous route.

## 2.2 Preparation of biomaterials by the non-hydrolytic sol-gel process

The non-hydrolytic sol-gel process is another route for the production of materials for bioapplications such as dental and osseous substitutes. Here the preparation and characterization of the glass ionomer by this methodology is described. Calcium fluoroaluminosilicate glass containing phosphorus and sodium (Ca-FAlSi) consists of an inorganic polymeric network (mixed oxide) embedded in an aluminum and silicon matrix, comprising an amorphous structure. This material is currently employed in dentistry as restorative designated glass ionomer cement [76, 77]. Firstly, the calcium-fluoroaluminosilicate glass was prepared in oven-dried glassware and  $\text{AlCl}_3$ ,  $\text{SiCl}_4$ ,  $\text{CaF}_2$ ,  $\text{AlF}_3$ ,  $\text{NaF}$ ,  $\text{AlPO}_4$ , and ethanol were reacted in reflux under argon atmosphere [53]. The  $^{27}\text{Al}$  NMR results revealed the coordination of aluminum. Figure 13 shows the NMR spectrum of the calcium-fluoroaluminosilicate glass dried at  $50^\circ\text{C}$  and submitted to heat treatment at  $1000^\circ\text{C}$ .

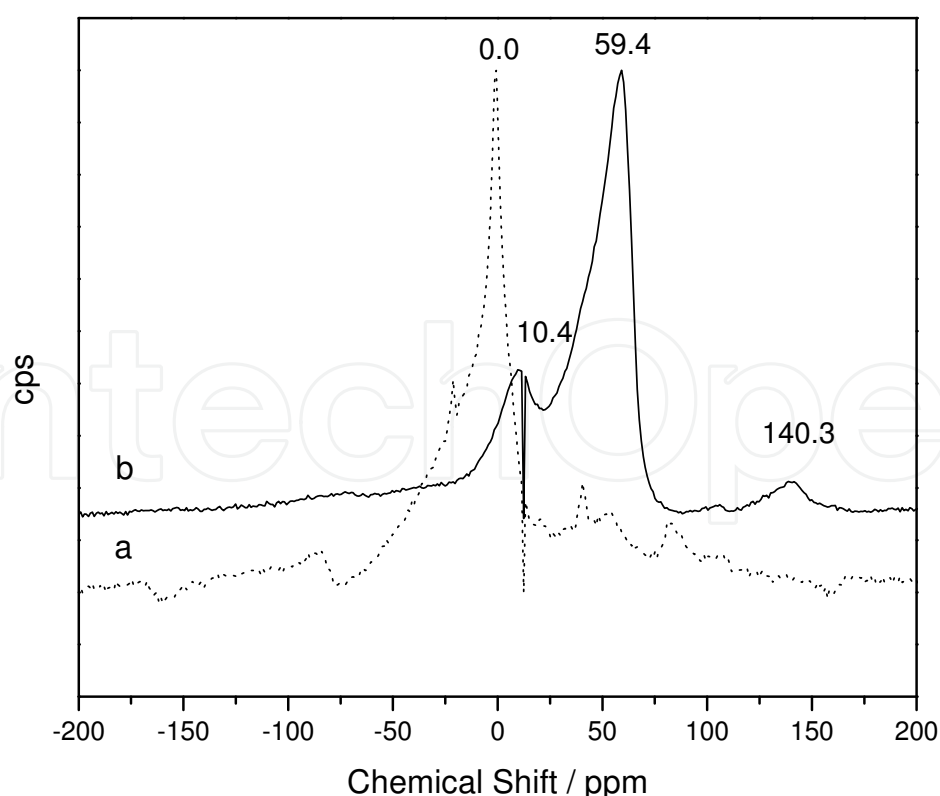


Fig. 13.  $^{27}\text{Al}$  NMR spectrum of the sample dried at  $50^\circ\text{C}$  and treated at  $1000^\circ\text{C}$ .

The central transition (CT) frequency of the spectrum of a quadrupolar nucleus of half integer spin, such as  $^{27}\text{Al}$  ( $I = 5/2$ ), depends on the orientation of each crystallite in the static magnetic field to the second order in the perturbation theory. The quadrupolar interaction between the nuclear electric quadrupole moment ( $eQ$ ) and the electric field gradient of the nucleus ( $eq$ ), arising from any lack of symmetry in the local electron distribution, is described by the quadrupolar coupling constant  $Cq$  ( $e^2qQ/h$ ) and the symmetry parameter  $\eta$ . It should be noted that disordered materials such as glasses have a wide range of interatomic distances and, consequently, CT line broadening occurs due to the distribution of  $\delta_{\text{iso}}$  and quadrupolar interactions [78]. After the material was heat-treated at  $1000^\circ\text{C}$ , a single peak corresponding to  $\text{Al}^{(\text{VI})}$  predominated at 0.0 ppm, indicating the structural change in the coordination state of aluminum. When Al atoms are in tetrahedral coordination  $\text{Al}^{(\text{IV})}$ , their chemical shifts vary from 55 to 80 ppm. Chemical shifts in the range of -10 to 10 ppm correspond to coordinated octahedral  $\text{Al}^{(\text{VI})}$  [79, 80, 47]. The spectra of the two samples prepared here presented three peaks at 10.4, 59.4, and 140.1 ppm, which are characteristic of  $\text{Al}^{(\text{VI})}$ ,  $\text{Al}^{(\text{IV})}$ , and spinning side bands [81], respectively. Although some authors have reported the presence of  $\text{Al}^{(\text{V})}$  atoms with chemical shifts at 20 ppm [82], this peak was not detected. The dominant species in the sample heat-treated at  $50^\circ\text{C}$  corresponded to  $\text{Al}^{(\text{IV})}$ . The chemical shifts between 50 and 60 ppm corresponding to  $\text{Al}^{(\text{IV})}$  depend on the Al/P molar ratio.  $\text{Al}^{(\text{IV})}$  has been found at 60 ppm in model glasses based on  $\text{SiO}_2\text{Al}_2\text{O}_3\text{CaOCaF}_2$ , and at about 50 ppm in glasses containing phosphate where the molar Al:P ratio was 2:1 [81]. In this study an Al/P molar ratio of approximately 10 was achieved, which is higher than that present in commercial glasses. In our case, this chemical shift was very difficult to observe because of the lower incidence of Al-O-P bonds. The  $^{29}\text{Si}$  NMR results allow for analysis of the chemical environment around silicon atoms in silicates, where Si is bound to four oxygen atoms. The structure around Si can be represented by a tetrahedron whose corners link to other tetrahedra. The  $Q^n$  notation serves to describe the substitution pattern around a specific silicon atom, with Q representing a silicon atom surrounded by four oxygen atoms and  $n$  indicating the connectivity [83]. Figure 14 presents the NMR spectrum of the sample dried at  $50^\circ\text{C}$ .

The material displayed a peak at -100 ppm and a shoulder at -110 ppm, and the values in this range were attributed to Si atoms  $Q^4$  and  $Q^4$  or  $Q^3$ , respectively. Figure 15 illustrates the  $Q^3$  and  $Q^4$  structure.

As mentioned above, the chemical shift indicates the environment around the Si atoms in the glass. The commercial calcium-fluoroaluminosilicate glass presents a broad peak between -90 and -99 ppm [82]. On the basis of the results obtained here, our material exhibits a vitreous lattice. The number of nearest neighbor aluminum atoms is given in parentheses.  $Q^4$  (3/4 Al) and  $Q^4$ (1/2) [78] are the structures represented in Figure 16.

The chemical shift ranges overlap, so the resonances in Fuji II cement (commercial glass) at -87, -92, -99, and -109 ppm may be due to  $Q^4$  (3/4 Al),  $Q^4$  (3 Al),  $Q^4$  (1/2 Al), and  $Q^4$  (0 Al), respectively [78]. In our case, the chemical shifts at -110 and 100 ppm may be due to the Si atoms  $Q^4$  (1/2 Al) and  $Q^4$  (0 Al), because of the molar ratio  $\text{Al}/\text{Si} < 1$ . Figure 17 illustrates the  $^{29}\text{Si}$  NMR of the sample heat-treated at  $1000^\circ\text{C}$  for 4 hours.

In the present case, only one peak at -88 ppm was detected, which can be attributed to the presence of a  $Q^4$  (3/4 Al) site in Si atoms due to the structural rearrangement of the



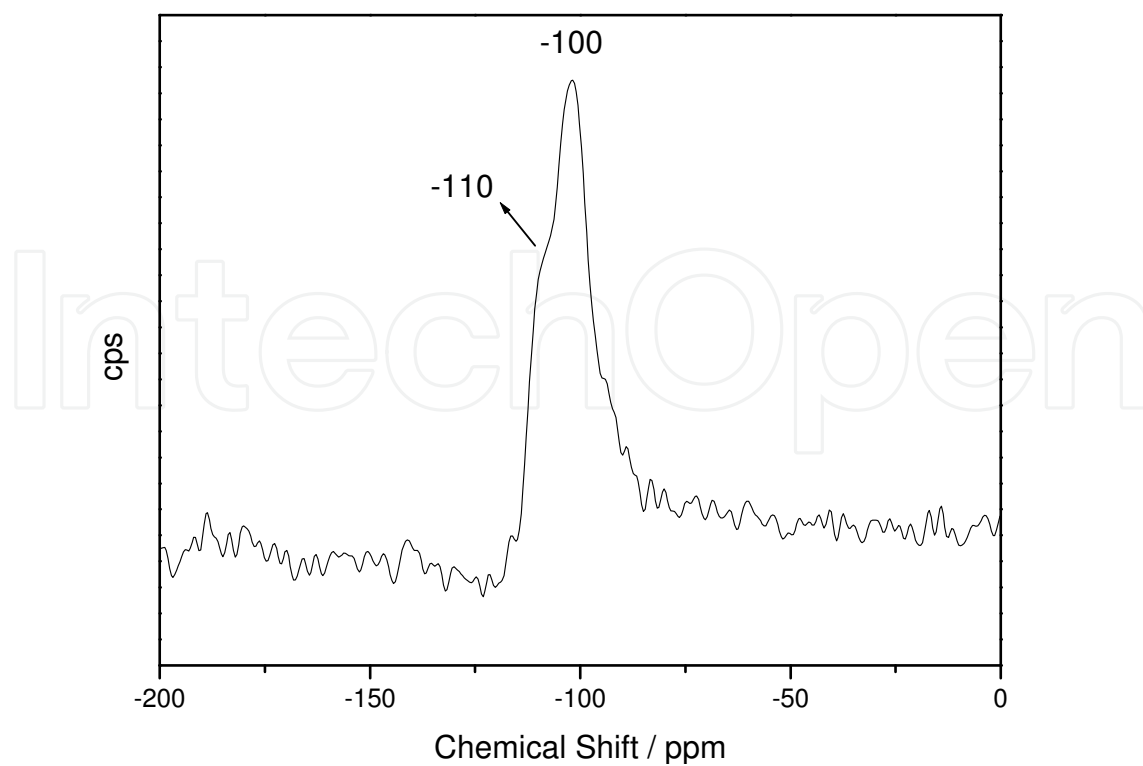


Fig. 14.  $^{29}\text{Si}$  NMR spectrum of the sample dried at  $50^\circ\text{C}$ .

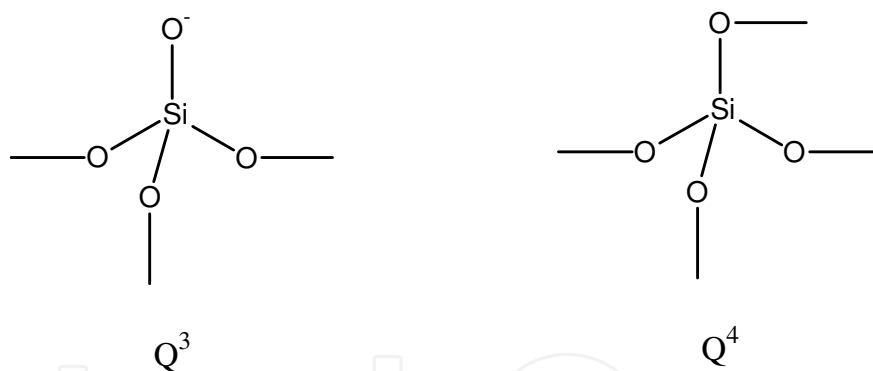


Fig. 15. Schematic representation of the  $\text{Q}^3$  and  $\text{Q}^4$  structures.

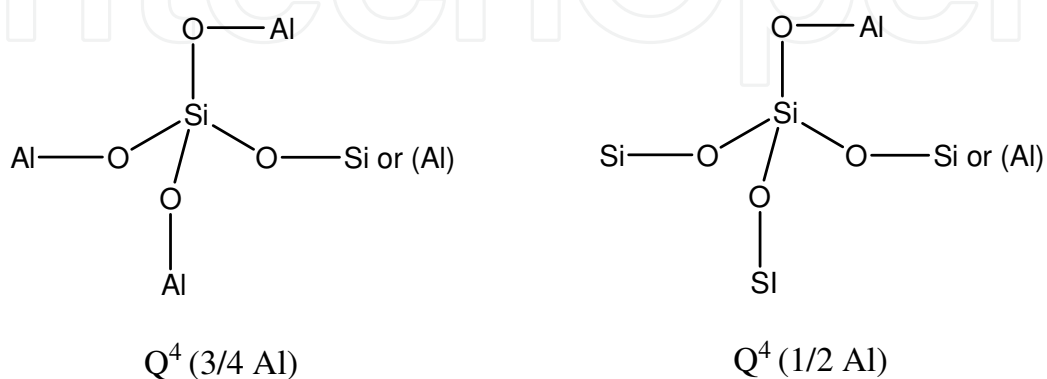


Fig. 16. Schematic representation of the  $\text{Q}^4 (3/4 \text{ Al})$  and  $\text{Q}^4 (1/2 \text{ Al})$  structure.

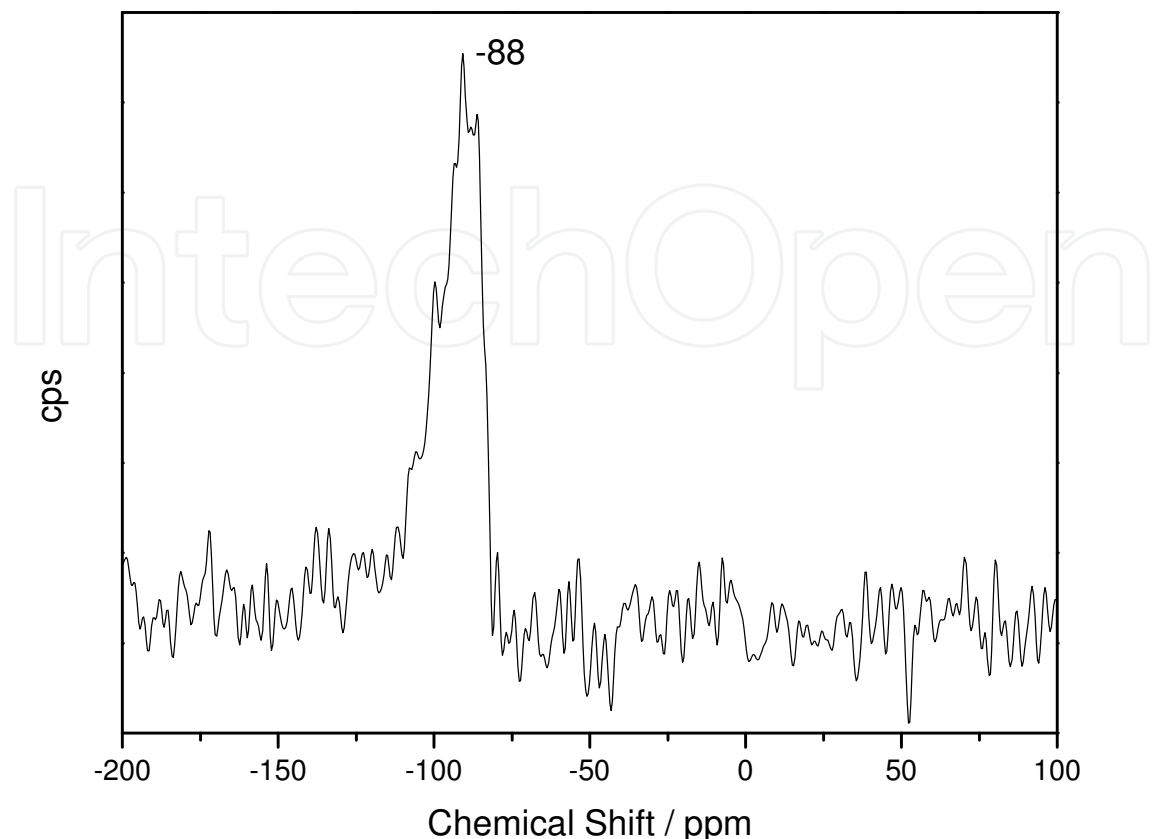


Fig. 17.  $^{29}\text{Si}$  NMR spectrum of the sample treated at  $1000^\circ\text{C}$ .

aluminosilicate crystalline structures. This is consistent with our X-ray data. The nonhydrolytic sol-gel method has proved efficient for the preparation of materials with glass properties, as shown in this work. This process enables reaction control and the use of stoichiometric amounts of Al and Si reagents at low temperatures, near  $110^\circ\text{C}$ , thereby reducing production costs.

The preparation of aluminosilicate-based matrices by the nonhydrolytic sol-gel method, using varying concentrations of the glass components, especially the element phosphorus, has been accomplished by our group [84]. Figure 18 depicts the X-ray diffractograms for the samples A2, A3.3, and A4, all dried at  $50^\circ\text{C}$ .

An amorphous structure predominates in sample A2. The A3.3 material displays an amorphous structure with crystalline phases attributed to fluorapatite ( $\text{Ca}_5(\text{PO}_4)_3\text{OH}$ ) and mullite ( $3\text{Al}_2\text{O}_3\cdot 2\text{SiO}_2$ ), according to Gorman et al. Sample A4 also presents an amorphous phase and a crystalline phase, which is ascribed to mullite [85]. The X-ray diffraction analysis revealed the influence of the phosphorus concentration on the structural formation of the materials. The material prepared with the Wilson formulation has an amorphous structure, while the one prepared according to Hill displays an amorphous structure with a crystalline phase attributed to mullite. An increase in phosphorus in the Hill formulation allows the formation of an amorphous material with crystalline phases attributed to mullite and fluorapatite. The increase in phosphorus concentration affects the formation of the

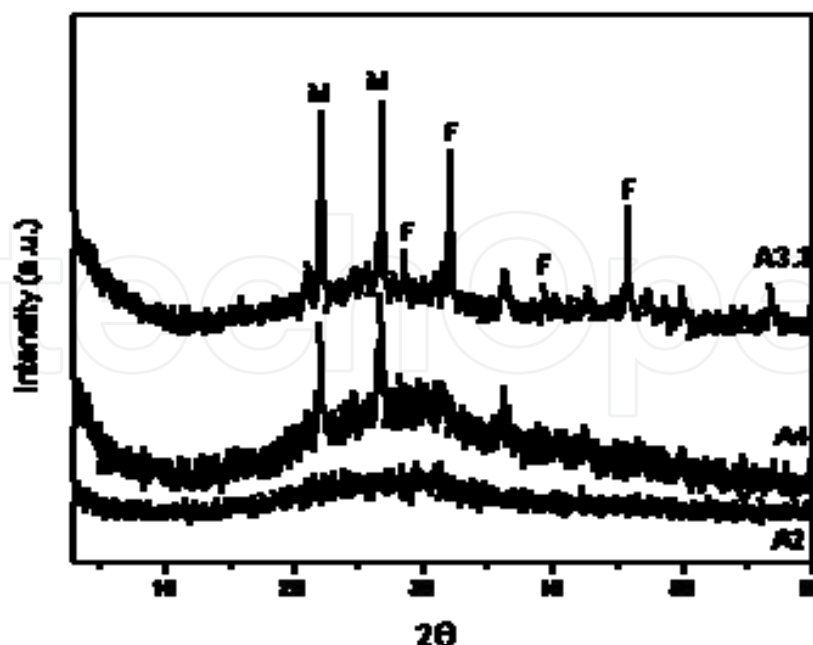


Fig. 18. X-ray diffractograms of samples A2, A3.3, and A4.

material's structure, since this increase leads to the formation of fluorapatite. The difference between the Wilson and Hill formulations [86, 87] also account for the formation of different materials: sample A2 material presents a structure devoid of crystallinity, while the structure of glass A4 contains a crystalline phase attributed to mullite. These are attractive factors in dental restorations. Calcium fluoroaluminosilicate glasses containing sodium and phosphorus are materials that can be employed in dentistry, as components of glass ionomer cement, and in medicine, as replacements for bone implants.

In this work, the preparation and characterization of matrices based on aluminosilicates obtained by the non-hydrolytic and hydrolytic sol-gel routes were investigated. Three different routes, namely the non-hydrolytic sol-gel route and the hydrolytic sol-gel route using either basic or acid catalysis, were employed in the preparation of three materials, namely IC1, IC2, and IC3. The obtained materials were characterized by different physical methods and antimicrobial activity tests. For evaluation of the antimicrobial activity, the materials were examined against the microorganisms *E. faecalis*, *S. salivarius*, *S. sobrinus*, *S. sanguinis*, *S. mutans*, *S. mitis*, and *L. casie*, using the double layer diffusion technique.

Scanning electron microscopy analysis coupled with energy dispersive spectroscopy (MEV/EDS) of the material IC1 (Figure 19) mapped the elemental distribution and showed that the silicon atoms are located in the same regions as the aluminum and oxygen atoms distributed throughout the particle surface. This indicates the possible formation of aluminosilicate, confirming the IR data. The presence of chlorine is evidence that this material contains a large amount of residual groups from the reagent  $\text{AlCl}_3$ . The calcium atoms are distributed over the IC1 matrix, but they appear as some clusters that coincide with the fluoride clusters, thereby indicating the presence of  $\text{CaF}_2$  crystals, as shown by XRD.

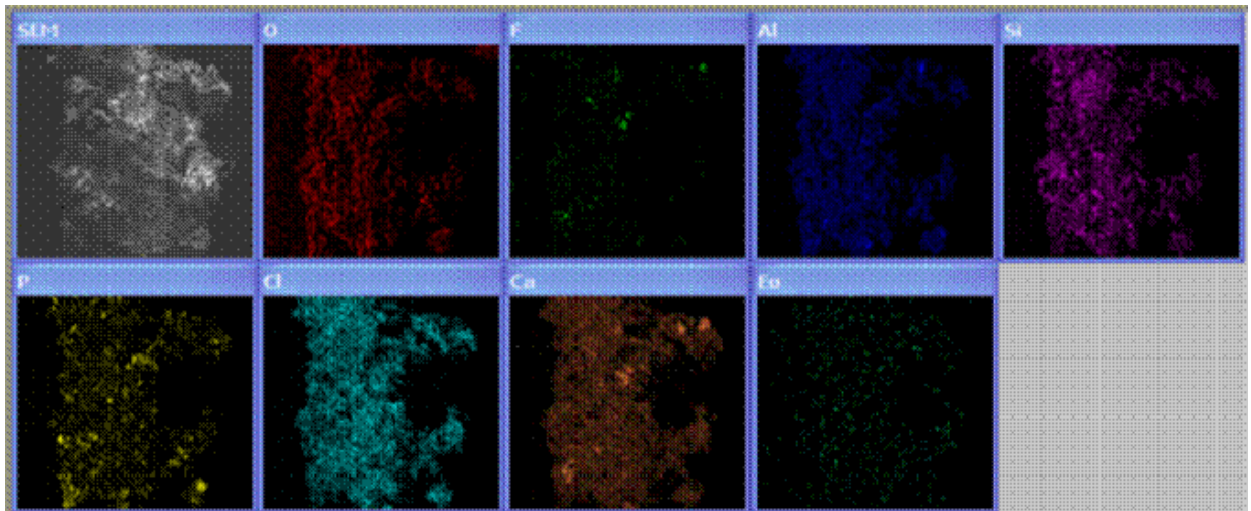


Fig. 19. Elemental distribution mapping of the material IC1 treated at 110 °C.

For the material IC2, the MEV/EDS analysis (Figure 20) revealed that the silicon atoms are located in the same regions as the aluminum and oxygen atoms, pointing to the possible formation of aluminosilicate. The smaller amount of chlorine in relation to IC1 indicates that this material has fewer residues, probably originated from the catalyst (HCl). Also, it is important to bear in mind that in this case the precursor  $\text{AlCl}_3$  was replaced with aluminum isopropoxide, which may be contributing to the lower amount of residual Cl groups. The phosphorus and calcium atoms are distributed over the matrix. This material contained no calcium and fluoride clusters, corroborating the XRD findings, which had not indicated the presence of  $\text{CaF}_2$ .

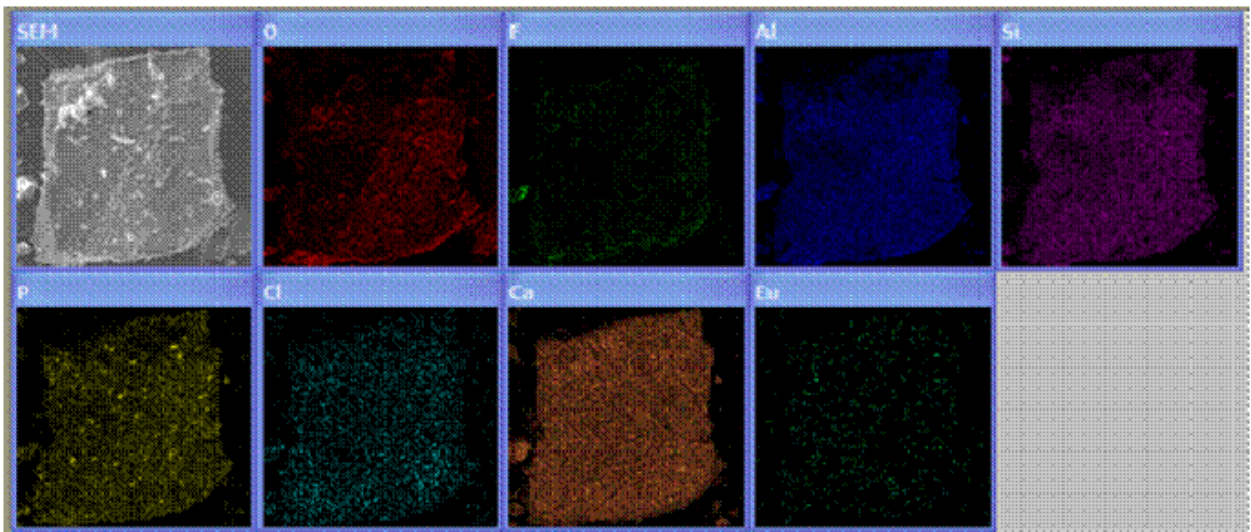


Fig. 20. Elemental distribution mapping of the material IC2 treated at 110 °C.

In the case of the material IC3, the MEV/EDS (Figure 21) demonstrated that the silicon atoms are present in the same regions as the aluminum and oxygen atoms. The smaller amount of chlorine in relation to IC2 indicates that this material has few residual Cl. The calcium atoms are distributed in the matrix and appear as clusters in the same regions as the fluoride atoms, indicating the presence of  $\text{CaF}_2$ , as previously detected by XRD.

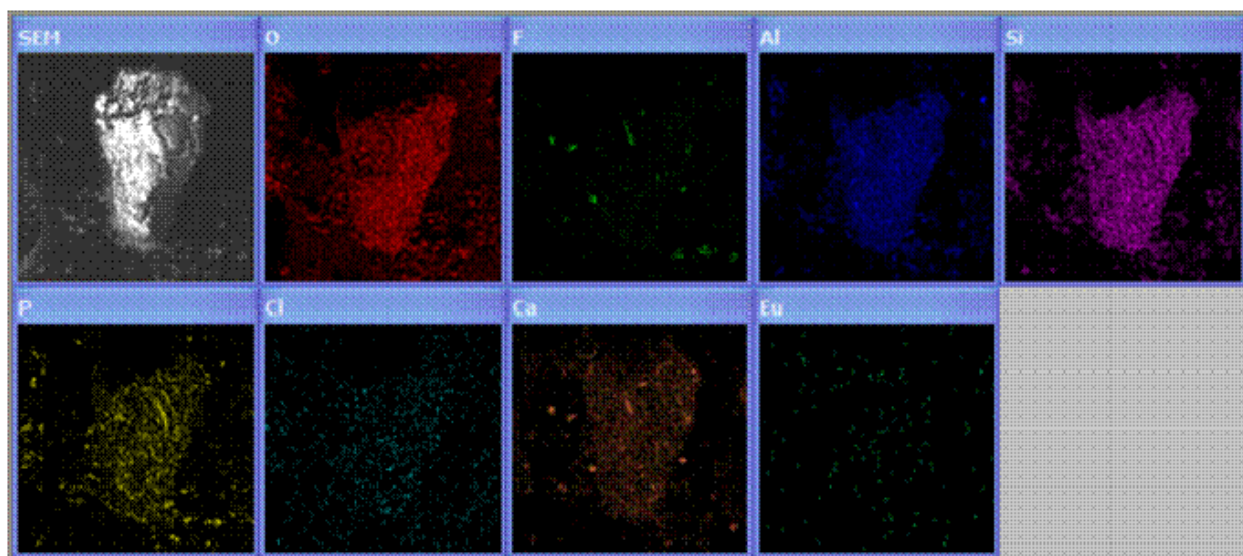


Fig. 21. Elemental distribution mapping of the material IC3.

The Ca-FAISi used as a basis for glass ionomer almost always presents amorphous phase separation. For instance, materials obtained by the usual methods are composed by distinct regions with high Al and Si content as well as other regions containing Ca, P, and F. This fact undermines the homogeneity of the Ca-FAISi material and impairs the setting reaction of the cement, because regions rich in Ca, P, and F are less reactive, which in turn promotes formation of inhomogeneous cement. This ruins the integrity of the restorative material and affects its physical and chemical resistance. In our case, there was no clear evidence of phase separation for the materials synthesized by the sol-gel methods, and the elements were well distributed on the surface of materials. The material IC2 presented high homogeneity compared to the other materials, since the elements were well distributed across the surface of the particles.

For evaluation of the antimicrobial activity of the materials prepared here, the dual layer diffusion technique was employed, using the microorganisms listed in Table 1.

The materials IC1 and IC2 presented antimicrobial activity similar to that of the commercial glass ionomer Ca-FAISi, so they can be applied in the oral environment and avoid damage by microorganisms. In conclusion, the material IC2 can be used as a basis for glass ionomer cement and the fact that it is synthesized at lower temperature and leads to greater homogeneity compared with the Ca-FAISi produced by industrial methods makes it advantageous over the commercially available materials.

The glass ionomer prepared in reference [84] was tested with respect to its biocompatible properties and compared to the materials obtained by the industrial methodology. Experimental and conventional GIC were analyzed in terms of morphology and of the morphometric reaction induced by the cement in the subcutaneous tissue of rats.

The methodology described in [88] was used for the biocompatible test. Table 2 lists the tested materials.

The experimental and conventional GIC powders were used to prepare the glass ionomer cement. The surface of the obtained materials was examined by scanning electron microscopy (Figures 22 a and b, respectively).



microorganism/ ATCC	Substance ( ) Extract ( ) Product (x)	Mean (mm) ± SD
E. faecalis ATCC 4082	IC 1	20.0
	IC 22x d	15.5 ± 2.1
	IC 3	0.0
	Gass ionomer (S.S. White Artigos Dentários LTDA)	22.0 ± 0.0
	Periorgard mouthwash (positive control)	13.0 ± 0.0
S. salivarius ATCC 25975	IC 1	18.0
	IC 22x d	12.0 ± 1.4
	IC 3	0.0
	Gass ionomer (S.S. White Artigos Dentários LTDA)	25.5 ± 0.7
	Periorgard mouthwash (positive control)	19.0 ± 0.0
S. sobrinuns ATCC 33478	IC 1	19.0
	IC 22x d	14.0 ± 1.4
	IC 3	0.0
	Gass ionomer (S.S. White Artigos Dentários LTDA)	9.5 ± 0.7
	Periorgard mouthwash (positive control)	21.0 ± 0.0
S. sanguinis ATCC 10556	IC 1	14.0
	IC 22x d	12.0 ± 2.8
	IC 3	0.0
	Gass ionomer (S.S. White Artigos Dentários LTDA)	10.5 ± 0.7
	Periorgard mouthwash (positive control)	18.0 ± 0.0
S. mutans ATCC 25175	IC 1	20.0
	IC 22x d	10.0 ± 2.8
	IC 3	0.0
	Gass ionomer (S.S. White Artigos Dentários LTDA)	10.0 ± 0.0
	Periorgard mouthwash (positive control)	21.5 ± 0.7
S. mitis ATCC 49456	IC 1	20.0
	IC 22x d	13.0 ± 2.8
	IC 3	0.0
	Gass ionomer (S.S. White Artigos Dentários LTDA)	14.0 ± 0.0
	Periorgard mouthwash (positive control)	18.5 ± 0.0
L. casei ATCC 11578	IC 1	19.0
	IC 22x d	16.0 ± 1.4
	IC 3	0.0
	Gass ionomer (S.S. White Artigos Dentários LTDA)	20.5 ± 0.7
	Periorgard mouthwash (positive control)	23.5 ± 0.7

Table 1. Antimicrobial activity tests for the materials prepared in this work.

GIC	Composition	Source
Experimental	Powder: Calcium fluoraluminiosilicates containing phosphorus and sodium	Sol-Gel Methodology
	Liquid: Tartaric acid, polyacrilic acid, distilled water	
Conventional (Vidrion R)	Powder: Sodium fluorosilicates, calcium aluminium, barium sulphate, pigments. Liquid: Tartaric acid, polyacrilic acid, destilled water	SS White - Prima Dental Group, Gloucester, UK

Table 2. Tested materials.



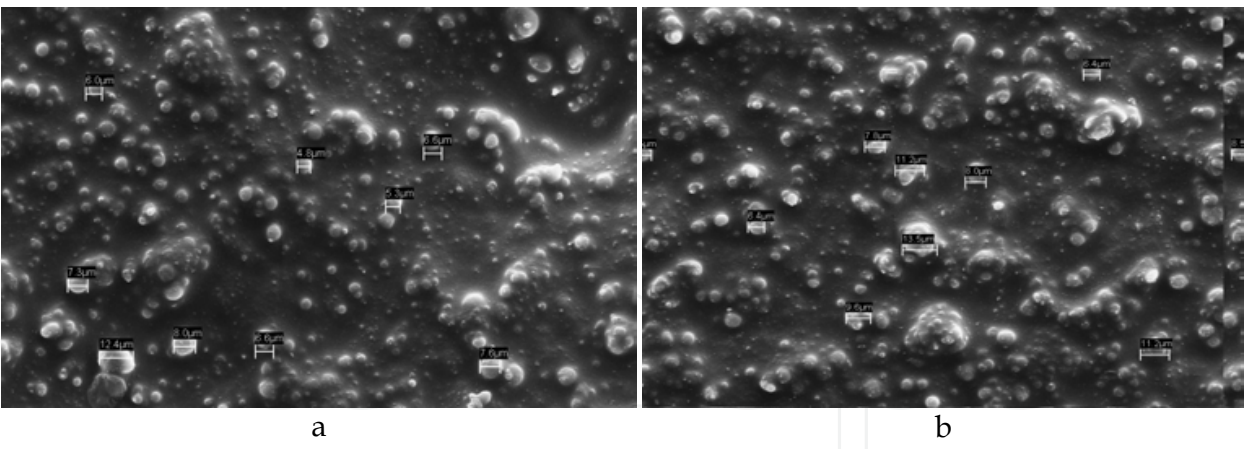


Fig. 22. SEM micrographs recorded for the glass ionomer cements. (a) experimental and (b) conventional

The micrographs revealed that the surface the conventional cement presents lower homogeneity, compared to the experimental cement. The better homogeneity of the experimental cement is due to the homogeneity of particle size, which promotes the same physical-chemistry properties all over the cement surface.

The biocompatible test was carried out on the basis of the response obtained with the tissue stimulated by the experimental cement and compared to that achieved with the conventional cement. These responses were analyzed by means of morphological and morphometric analyses of the reaction caused by these cements in the subcutaneous tissue of rats. Polyethylene tubes were obtained according to the methodology used by Campos-Pinto et al. [89]. To this end, an urethral catheter with an internal diameter of 0.8 mm was sectioned sequentially at 10 mm intervals. After sectioning, one of the tube ends was sealed with cyanoacrylate ester gel (Super Bonder, Aachen, Germany), to avoid extravasation of the material to be tested. The obtained tubes were placed in a metal box and autoclaved at 120°C for 20 min. [90].

The data obtained for all the histopathological events assessed in each period of study are presented in Table 3.

Histopathological Events	7 days			21 days			42 days		
	GGI	GGII	CCG	GGI	GGII	CCG	GGI	GGII	CCG
Polymorphonuclear	+++	+++	++	++	++	++	--	--	--
Mononuclear	+++	++++	++	++	++	++	--	--	--
Fibroblasts	+++	+++	++	++	++	++	++	++	++
Blood vessels	+++	++++	+++	+++	++	++	++	++	--
Macrophage	++	+++	++	--	++	--	--	--	--
Giant inflammatory cells	++	++	++	--	--	--	--	--	--

Score: (-) absent; (+) slight; (++) moderate; (+++) intense.  
CG - control group; GI - experimental cement; GII - conventional cement.

Table 3. Summary of the data obtained for the histopathological events observed in each group at the different periods of study.

Figures 23, 24, and 25 show the biocompatible tests after 7, 21, and 42 days, respectively.

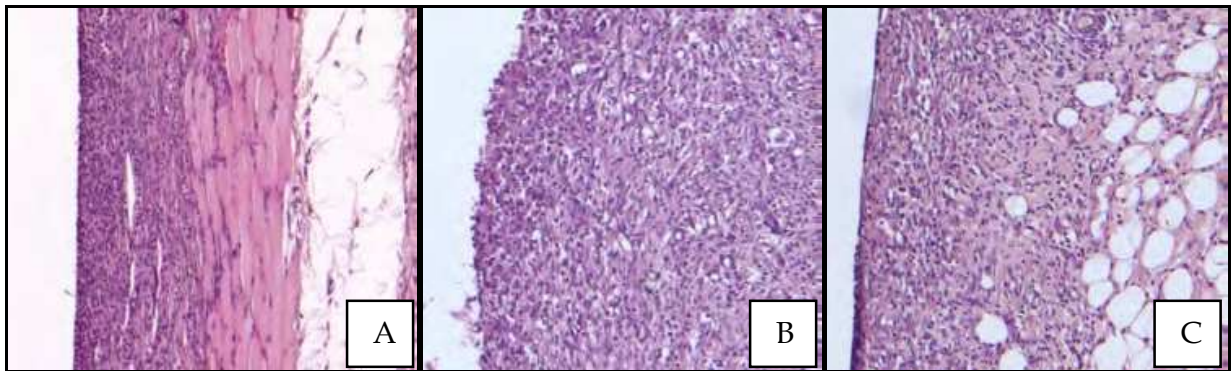


Fig. 23. Biocompatible tests after 7 days. Control group (A), conventional GIC (B), and experimental GIC (C) (100X. H.E.).

In the case of the control group (CG), connective tissue with delicate fibers, highly cellularized with fibroblasts and several blood vessels adjacent to all the analyzed faces was observed after 7 days (Figure 23A). A mild chronic inflammatory reaction was also detected. As for the experimental cement group (GI) (Experimental GIC), a layer of cellularized connective tissue with moderate chronic inflammatory reaction, predominantly formed by lymphocytes and blood vessels, was observed after 7 days. Small areas of necrosis were also noted (Fig. 23B). Few macrophages or foreign body multinucleated giant cells were seen. Concerning the conventional cement (GII) (Conventional GIC), an intense chronic inflammatory reaction, associated with hyperemic blood vessels and macrophages (Figure 23C) was detected after 7 days. Necrosis area was observed close to the dispersed material.

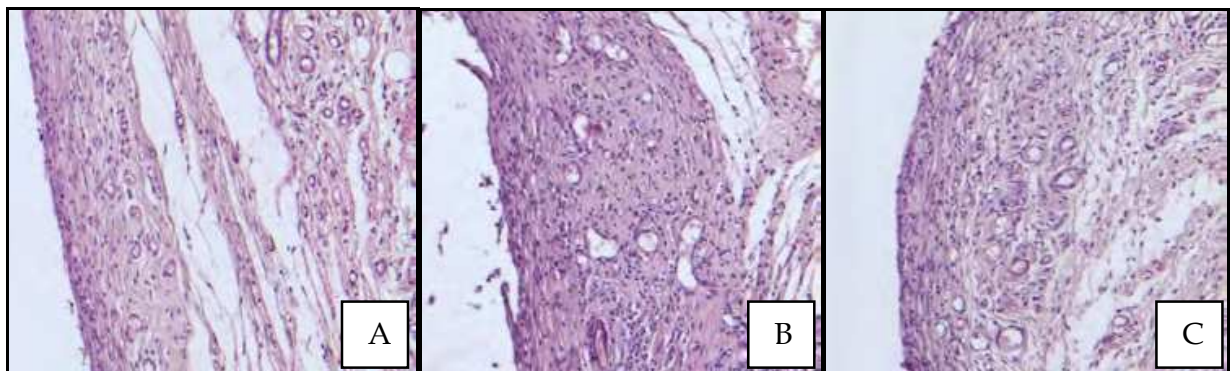


Fig. 24. Biocompatible tests after 21 days. Control group (A), conventional GIC (B), and experimental GIC (C) (100X. H.E.).

After 21 days, the CG group presented a mild chronic inflammatory reaction in this period (Figure 24A). As for GI (Experimental GIC), there was a mild chronic inflammatory reaction, with few lymphocytes and several fibroblasts, in the connective tissue adjacent to the open end of the tube. Foreign body multinucleated giant cells and macrophages were not observed (Figure 24B). In the case of GII (Conventional GIC), the connective tissue exhibited a moderate chronic inflammatory reaction. Phagocytic activity and rare necrosis areas were also observed (Figure 24C).

After 42 days, the CG presented no chronic inflammatory reaction (Figure 25A). Concerning the GI group (Experimental GIC), connective tissue with mild to absent chronic

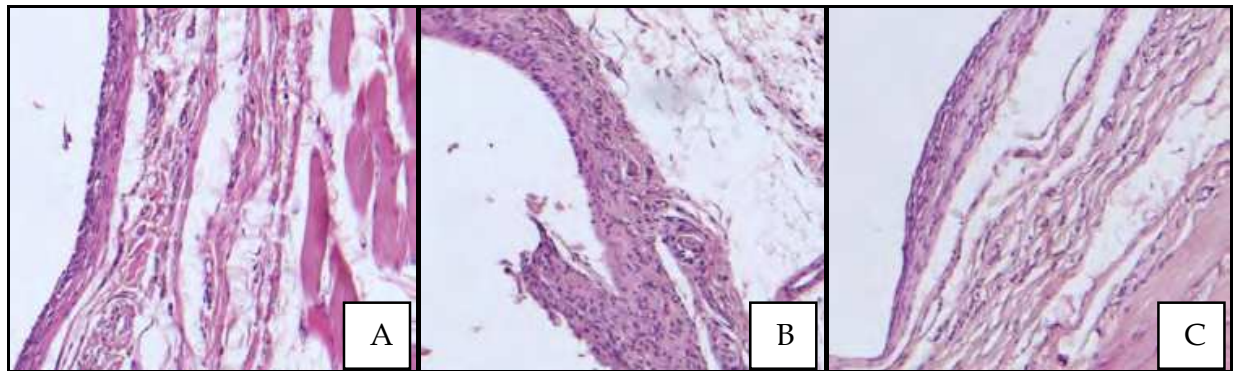


Fig. 25. Biocompatible tests after 42 days. Control group (A), conventional GIC (B), and experimental GIC (C) (100X. H.E.).

inflammatory reaction and residual dispersed cement was detected (Figure 25B), while necrosis areas and other changes were absent. As for GII (Conventional GIC), there was a mild to absent chronic inflammatory reaction, without foreign body giant cells or macrophages. Some dispersed material was observed, but no necrosis areas or degenerative changes were seen (Figure 25C).

In summary, both tested cements caused a mild to absent inflammatory response after 42 days, which is also acceptable from a biological standpoint.

### 3. Conclusion

Bioapplications that could provide better quality of life for humanity are desirable. It has been demonstrated here that a series of materials prepared by sol-gel methodology (hydrolytic and non-hydrolytic routes) present useful properties for application in biological medium. Indeed, it was possible to obtain multifunctional materials by this methodology. The combination of the different elements at molecular and atomic level affords potential candidates for a variety of applications. The very interesting results obtained by us in the present work indicate that this methodology can be applied for production of biomaterials with potential application in several fields such as medicine, dentistry, veterinary, engineering, chemistry, physics, and biology. Materials for use in the areas of bone implant, restorative tooth coating, diagnosis, membrane permeability, biosensor, scaffolding, and drug delivery can be prepared and transformed into biocompatible, bioactive, bioinducer materials with different properties and composition, since this methodology allows for production of materials with controlled stoichiometry and particle size.

### 4. Acknowledgment

The authors gratefully acknowledge the financial support of the Brazilian research funding agencies FAPESP, CNPq, and CAPES. Profa. Dra. Isabel Salvado from Departamento de Engenharia Cerâmica e do Vidro - CICECO - Universidade de Aveiro/Pt, Dr. Jorge V. L. Silva do Centro da Tecnologia da Informação Renato Archer (CTI), - Campinas - SP - Brazil, Profa. Dra. Shirley Nakagaki, Departamento de Química da Universidade Federal do Paraná - PR - Brazil, Profa. Dra. Fernanda de C. P. Pires de Souza, Departamento de Materiais Dentários da Universidade de São Paulo - Ribeirão Preto - SP - Brazil, and Prof. Dr. Carlos Henrique Martins da Universidade de Franca - Franca - SP - Brazil are also acknowledged.



## 5. References

- [1] Nair, L. S., Laurencin, C. T. (2006). Polymers as Biomaterials for Tissue Engineering and Controlled Drug Delivery, *Adv Biochem Engin/Biotechnol*, Vol. 102, pp. 47-90.
- [2] Hench, L. L. (1998), .Biomaterials: a forecast for the future.. *Biomaterials*, Vol. 19, No 16, pp. 1419-1423.
- [3] Leeuwenburgh, S. C. G., Malda, J., Rouwkema, J., Kirkpatrick, C. J. (2008). Trends in biomaterials research: An analysis of the scientific programme of the World Biomaterials Congress 2008. *Biomaterials*, Vol. 29, pp. 3047-3052.
- [4] Bonzani, I. C. , Adhikari, R., Houshyar, S., Mayadunne, R., Gunatillake, P., Stevens, M. M. (2007). Synthesis of two-component injectable polyurethanes for bone tissue engineering. *Biomaterials*, Vol. 28, No 3, pp. 423-433.
- [5] Balani, K., Anderson, R., Laha, T., Andara, M., Tercero, J., Crumpler, E., Agarwal, A. (2007). Plasma-sprayed carbon nanotube reinforced hydroxyapatite coatings and their interaction with human osteoblasts in vitro. *Biomaterials*, Vol. 28, No 3, pp. 618-624.
- [6] Chu, T. M. G., Warden, S. J., Turner, C. H., Stewart, R. L. (2007). Segmental bone regeneration using a load-bearing biodegradable carrier of bone morphogenetic protein-2. *Biomaterials*, Vol. 28, No. 3, pp. 459-467.
- [7] Eglin, D., Maalheem, S., Livage, J., Coradin, T. (2006). In vitro apatite forming ability of type I collagen hydrogels containinrg bioactive glass and silica sol-gel particles. *J. Mat Scie. Mat In Medicine*, Vol. 17, No. 2, pp. 161-167.
- [8] Skelton, K. L., Glenn, J. V., Clarke, S. A., Georgiou, G., Valappil, S. P., Knowles, J. C., Nazhat, S. N., Jordan, G. R. (2007). Effect of ternary phosphate-based glass compositions on osteoblast and osteoblast-like proliferation, differentiation and death in vitro. *Acta Biomaterialia*, Vol. 3, No. 4, pp. 563-572.
- [9] Misra, S. K., Mohn, D., Brunner, T. J., Stark, W. J., Philip, S. E., Roy, I., Salih, V., Knowles, J. C., Boccaccini, A. R. (2008). Comparison of nanoscale and microscale bioactive glass on the properties of P(3HB)/Bioglass® composites. *Biomaterials*, Vol. 29, No. 12, pp. 1750-1761.
- [10] Lee, H. J., Choi, H. W., Kim, K. J., Lee, S. C. (2006). Modification of Hydroxyapatite Nanosurfaces for Enhanced Colloidal Stability and Improved Interfacial Adhesion in Nanocomposites, *Chem. Mater.*, Vol. 18, pp. 5111-5118.
- [11] Rámila, A., Padilla, S., Muñoz, B., Regí, M. V. (2002). A New Hydroxyapatite/Glass Biphasic Material: In Vitro Bioactivity. *Chem. Mater.*, Vol. 14, pp. 2439-2443.
- [12] Doğan, O., Öner, M. (2006). Biomimetic Mineralization of Hydroxyapatite Crystals on the Copolymers of Vinylphosphonic Acid and 4-Vinylimidazole. *Langmuir*, Vol. 22, pp. 9671-9675.
- [13] Iwatsubo, T., Sumaru, K., Kanamori, T., Shinbo, T., Yamaguchi, T. (2006). Construction of a New Artificial Biomineralization System. *Biomacromolecules*, Vol. 7, pp. 95-100.
- [14] Clupper, D. C., Hench, L. L. (2003). Crystallization kinetics of tape cast bioactive glass 45S5. *J. Non-Cryst. Solids*, Vol. 318, No. 1-2, pp. 43-48.
- [15] Hench, L. L. (1997). Sol-gel materials for bioceramic applications. *Current Opinion in Solid State & Material Science*, Vol. 2, No 5, pp. 604-610.

- [16] Pickup, D. M., Speight, R. J., Knowles, J. C., Smith, M. E., Newport, R. J. (2008). Sol-gel synthesis and structural characterisation of binary  $\text{TiO}_2\text{-P}_2\text{O}_5$  glasses. *Mater. Research Bulletin*, Vol. 43, No. 2, pp. 333-342.
- [17] Carla, D., Pickup, D. M., Knowles, J. C., Ahmed, I., Smith, M. E., Newport, R. J. (2007). A structural study of sol-gel and melt-quenched phosphate-based glasses. *J. Non-Cryst. Solids*, Vol. 353, No. 18-21, pp. 1759-1765.
- [18] Saravanakumar, B., Rajkumar, M., Rajendran, V. (2011). Synthesis and characterisation of nanobioactive glass for biomedical applications, *Materials Letters*, Vol. 65, pp. 31-34.
- [19] Lei, B., Chen, X., Wang, Y., Zhao, N., Miao, G., Li, Z., Lin, C. (2010). Fabrication of porous bioactive glass particles by one step sintering, *Materials Letters*, Vol. 64, pp. 2293-2295.
- [20] Chen, Q.-Z., Li, Y., Jin, L.-Y., Quinn, J. M. W., Komesaroff, P. A. (2010). A new sol-gel process for producing  $\text{Na}_2\text{O}$ -containing bioactive glass ceramics, *Acta Biomaterialia*, Vol. 6, pp. 4143-4153.
- [21] Kokubo, T., Kim, H.-M., Kawashita, M. (2003). Novel bioactive materials with different mechanical properties, *Biomaterials*, Vol. 24, pp. 2161-2175.
- [22] Olmo, N., Martín, A. I., Salinas, A. J., Turnay, J., Vallet-Regí, M., Lizarbe, M. A. (2003). Bioactive sol-gel glasses with and without a hydroxycarbonate apatite layer as substrates for osteoblast cell adhesion and proliferation, *Biomaterials*, Vol. 24, pp. 3383-3393.
- [23] Vrancken, K. C., Possemiers, K., Voort, P. V. D., Vansant, E. F. (1995). Surface modification of silica gels with aminoorganosilanes *Colloids Surf. A: Physicochem. Eng. Aspects*, Vol. 98, No. 3, pp. 235-241.
- [24] Mark, J. E., Lee, C. Y. C., Bianconi, P. A., Hybrid Organic-Inorganic Composites. ISBN 9780841231481 (ACS Symp. Ser. 586, American Chemical Society Washington, DC, 1995).
- [25] Cerveau, G., Corriu, R. J. P., Lepeytre, C., Mutin, P. H. (1998). Influence of the nature of the organic precursor on the textural and chemical properties of silsesquioxane materials *J. Mater. Chem.*, Vol. 12, No. 8, pp. 2707-2714.
- [26] Corriu, R. (1998). A new trend in metal-alkoxide chemistry: the elaboration of monophasic organic-inorganic hybrid materials. *Polyhedron*, Vol. 17, No. 5-6, pp. 925-934.
- [27] Corriu, R. J. P., Leclercq, D. (1996) Recent Developments of Molecular Chemistry for sol-gel Processes. *Angew Chem Int Engl.*, Vol. 35 No. 13-14, pp. 1420-1436.
- [28] Shea, K. J., Loy, D. A., Webster, O. (1992). Arylsilsesquioxane gels and related materials. New hybrids of organic and inorganic networks. *J Am Chem Soc.*, Vol. 114, No. 17, pp. 6700-6710.
- [29] Jackson, C. L., Bauer, B. J., Nakatami, A. I., Barnes, J. (1996). Synthesis of Hybrid Organic-Inorganic Materials from Interpenetrating Polymer Network Chemistry. *Chem. Mater.*, Vol. 8, No. 3, pp. 727-733.
- [30] Brinker, C. J.; Scherer, G. W. Sol-Gel Science, The Phys Chem. Sol-Gel Processing, ISBN 0121349705, Academic Press, San Diego, 1990.
- [31] Nassar, E. J., Ciuffi, K. J., Ribeiro, S. J. L., Messaddeq, Y. (2003). Europium incorporated in the silica matrix obtained by sol-gel methodoly: Luminescent materials *Mater Research*, Vol. 6, No 4, pp. 557-562.

- [32] Beari, F., Brand, M., Jenkner, P., Lehnert, R., Metternich, H. J., Monkiewicz, J., Siesler, H. W. (2001), Organofunctional alkoxysilanes in dilute aqueous solution: new accounts on the dynamic structural mutability. *J. Organo Chem.*, Vol. 625, No. 2, pp. 208-216.
- [33] Nassar, E. J., Neri, C. R., Calefi, P. S., Serra, O. A. (1999). Functionalized silica synthesized by sol-gel process. *J Non-Cryst Solids*, Vol. 247, No 1-3, pp. 124-128.
- [34] Stöber, W., Fink, A., Bohn, E. (1968). Controlled growth of monodisperse silica spheres in the micron size range. *J. Coll. Inter. Scie.*, Vol. 26, No. 1, pp. 62-69.
- [35] Papacídoro, A. T., Rocha, L. A., Caetano, B. L., Molina, E. F., Sacco, H. C., Nassar, E. J., Martinelli, Y., Mello, C., Nakagaki, S., Ciuffi, K. J. (2006). Preparation and characterization of spherical silica-porphyrin catalysts obtained by the sol-gel methodology. *Coll and Surfaces*, Vol. 275, No. 1-3, pp. 27-35.
- [36] Nassar, E. J., Nassor, E. C. O., Ávila, L. R., Pereira, P. F. S., Cestari, A., Luz, L. M., Ciuffi, K. J., Calefi, P. S. (2007). Spherical hybrid silica particles modified by methacrylate groups. *J. Sol-Gel Scie. Techn.*, Vol. 43, No. 1, pp. 21-26.
- [37] Ricci, G. P., Rocha, Z. N., Nakagaki, S., Castro, K. A. D. F., Crotti, A. E. M., Calefi, P. S., Nassar, E. J., Ciuffi, K. J. (2011). Iron-Alumina Materials Prepared by the Non-Hydrolytic Sol-Gel Route: Synthesis, Characterization and Application in Hydrocarbons Oxidation Using Hydrogen Peroxide as Oxidant, *Applied Catalysis A: General*, Vol. 389, No 1-2, pp. 147-154.
- [38] Matos, M. G., Pereira, P. F. S., Calefi, P. S., Ciuffi, K. J., Nassar, E. J. (2009). Preparation of a GdCaAl<sub>3</sub>O<sub>7</sub> Matrix by the non-hydrolytic sol-gel route. *Journal of Luminescence*, Vol. 129, pp. 1120-1124.
- [39] Langer, R. (2000). Biomaterials in Drug Delivery and Tissue Engineering: One Laboratory's Experience. *Acc. Chem. Res.*, Vol. 33, No. 2, pp. 94-101
- [40] Kumar, D. S., Banji, D., Madhavi, B., Bodanapu, V., Dondapati, S., Sri, A. P., (2009). Nanostructured porous silicon - a novel biomaterials for drug delivery. *International Journal of Pharmacy and Pharmaceutical Sciences*, Vol. 1, No 2, pp. 8-16
- [41] Arruebo, M., Galán, M., Navascués, N., Téllez, C., Marquina, C., Ibarra, M. R., and Santamaria, J. (2006). Development of Magnetic Nanostructured Silica-Based Materials as Potential Vectors for Drug-Delivery Applications. *Chem. Mater.*, Vol. 18, No. 7, pp. 1911-1919
- [42] Borak, B., Arkowski, J., Skrzypiec, M., Ziółkowski, P., Krajewska, B., Wawrzynska, M., Grotthus, B., Gliniak, H., Szlag, A., Mazurek, W., Biały, D., Maruszewsk, K., (2007). Behavior of silica particles introduced into an isolated rat heart as potential drug carriers. *Biomed. Mater.*, Vol. 2, No. 4, pp. 220-223.
- [43] Vallet-Regí, M., Balas, F., Arcos, D. (2007). Mesoporous Materials for Drug Delivery *Angew. Chem. Int. Ed.*, Vol. 46, pp. 7548-7558.
- [44] Yagüe, C., Moros, M., Grazú, V., Arruebo, M., Santamaría, J. (2008). Synthesis and stealthing study of bare and PEGylated silica micro- and nanoparticles as potential drug-delivery vectors., *Chemical Engineering Journal*, Vol. 137, No. 1, pp. 45-53.
- [45] Yang, J., Lee, J., Kang, J., Lee, K., Suh, J-S., Yoon, H-G., Huh, Y-M., Haam, S. (2008). Hollow Silica Nanocontainers as Drug Delivery Vehicles. *Langmuir.*, Vol. 24, No. 7, pp. 3417-3421.
- [46] Hench, L. L., West, J. K. (1990). The sol-gel process. *Chemical Reviews*, Vol. 90, No 1, pp. 33-72.



- [47] Acosta, S., Corriu, R. J. P., Leclercq, D., Lefevre, P., Mutin, P. H., Vioux, A. (1994). Preparation of alumina gels by a non-hydrolytic sol-gel processing method *J. Non-Cryst. Solids*, Vol. 170, No.3, 234-242.
- [48] Wright, J. D., Sommerdijk, N. A. J. (2003). *M. Sol-Gel Materials: Chemistry and Applications*; ISBN 90-5699-326-7; Taylor & Francis: London, Vol. 4.
- [49] Nassar, E. J., Ciuffi, K. J., Calefi, P. S. (2010). Europium III: different emission spectra in different matrices the same element, ISBN 978-1-61728-306-2. Chemistry Research and Applications, Editors: Harry K. Wright and Grace V. Edwards, Nova Science Publishers, Inc, New York, United State of America.
- [50] Bandeira, L. C., Ciuffi, K. J., Calefi, P. S., Nassar, E. J. (2010). Silica matrix doped with calcium and phosphate by sol-gel. *Advances Bioscience and Biotechnology*, Vol. 1, No. 3, pp. 200-207.
- [51] de Campos, B. M., Bandeira, L. C., Calefi, P. S., Ciuffi, K. J., Nassar, E. J., Silva, J. V. L., Oliveira, M., Maia, I. A. (2010). Protective coating materials on rapid prototyping by sol-gel, *Virtual and Physical Prototyping*, DOI: 10.1080/17452759.2010.491938. in press.
- [52] Pereira, P. F. S., Matos, M. G., Ávila, L. R., Nassor, E. C. O., Cestari, A., Ciuffi, K. J., Calefi, P. S., Nassar, E. J. (2010). Red, Green and Blue (RGD) Emission doped  $Y_3Al_5O_{12}$  (YAG) phosphors prepared by non-hydrolytic sol-gel route. *Journal of Luminescence*, Vol. 130, pp. 488-493.
- [53] Cestari, A., Avila, L. R., Nassor, E. C. O., Pereira, P. F. S., Calefi, P. S., Ciuffi, K. J., Nakagaki, S., Gomes, A. C. P., Nassar, E. J. (2009). Characterization Of Glass Ionomer Dental Cements Prepared By A Non-Hydrolytic Sol-Gel Route. *Materials Research*, Vol 12, no 2, pp. 139-143.
- [54] Nassar, E. J., Pereira, P. F. S., Ciuffi, K. J., Calefi, P. S. (2008). Photoluminescence Research Progress Chapter 10: Recent Development of Luminescent Materials Prepared by the Sol-Gel Process, 978-1-60456-538-6 Editors: Harry K. Wright and Grace V. Edwards, pp 265-285, Nova Science Publishers, Inc. New York, United State of America.
- [55] Bandeira, L. C., Calefi, P. S., Ciuffi, K. J., Nassar, E. J., Salvado, I. M. M., Fernandes, M. H. F. V. (2011) Low Temperature Synthesis of Bioactive Materials, *Cerâmica*, in press.
- [56] Kokubo, T. (1991). Bioactive glass ceramics: properties and applications, *Biomaterials*, Vol. 12, No 1, pp. 55-63.,
- [57] Villacampa A.I., Ruiz J.M.G. (2000). Synthesis of a new hydroxyapatite-silica composite material. *Journal of Crystal Growth*, Vol. 11, pp. 111-115.
- [58] Park, E., Condrate, R. A., Lee, D., Kociba, J., Gallagher, P. K. (2002). Characterization of hydroxyapatite: Before and after plasma spraying. *J. Mater. Sci.: Materials in Medicine*, Vol. 13, No. 2, 211-218.
- [59] Petil, O., Zanutto, E. D., Hench, L. L. (2001). Highly bioactive  $P_2O_5$ - $Na_2O$ - $CaO$ - $SiO_2$  glass-ceramics. *J. Non-Cryst. Solids*, Vol. 292, No. 1-3, pp. 115-126.
- [60] Li, J., Chem, Y., Yin, Y., Yao, F., Yao, K. (2007). Modulation of nano-hydroxyapatite size via formation on chitosan-gelatin network film in situ. *Biomaterials*, Vol. 28, No. 5, pp. 781-790.
- [61] Sachlos, E., Wahl, D. A., Triffitt, J. T., Czernuszka, J. T. (2008). The impact of critical point drying with liquid carbon dioxide on collagen-hydroxyapatite composite scaffolds, *Acta Biomaterialia*, Vol. 4, No. 5, pp. 1322-1331.

- [62] Liulan, L., Qingxi, H., Xianxu, H., Gaochun, H. (2007). Magnetic Properties and Intergranular Action in Bonded Hybrid Magnets, *J. Rare Earths*, Vol. 25, No. 3, pp. 336-340.
- [63] Sachlos, E., Reis, N., Ainsley, C., Derby, B., Czernuszka, J. T. (2003). Novel collagen scaffolds with predefined internal morphology made by solid freeform fabrication, *Biomaterials*, Vol. 24, No. 8, pp. 1487-1497.
- [64] Li, J., Habibovic, P., Yuan, H., van den Doel, M., Wilson, C. E., de Wijn, J. R., van Blitterswijk, C. A., de Groot, K. (2007). Biological performance in goats of a porous titanium alloy-biphasic calcium phosphate composite, *Biomaterials*, Vol. 28, No. 29, pp. 4209-4218.
- [65] Hollander, D. A., von Walter, M., Wirtz, T., Sellei, R., Schmidt-Rohlfing, B., Paar, O., Erli, H. (2006). Structural, mechanical and in vitro characterization of individually structured Ti-6Al-4V produced by direct laser forming, *Biomaterials*, Vol. 27, No. 7, pp. 955-963.
- [66] Lee, B. H., Abdullah, J., Khan, Z. A. (2005). Optimization of rapid prototyping parameters for production of flexible ABS object, *J. Mater. Processing Techn.*, Vol. 169, No. 1, pp. 54-61.
- [67] Mostafa, N., Syed, H. M., Igor, S., Andrew, G. (2009). Performance Comparison of IP- Networked Storage, *Tsinghua Scie. & Techn.*, Vol. 14, No. 1, pp. 29-40.
- [68] Galantucci, L. M., Lavecchia, F., Percoco, G. (2008). Study of compression properties of topologically optimized FDM made structured parts, *CIRP Annals – Manufacturing Techn.*, Vol. 57, No. 1, pp. 243-246.
- [69] Bandeira, L. C., Calefi, P. S., Ciuffi, K. J., Nassar, E. J., Salvado, I. M., Fernandes, M. H. F. V., Silva, J. V. L., Oliveira, M., Maia, I. A. (2011). Calcium Phosphate Coatings By Sol-Gel On Acrylonitrile-Butadiene-Styrene Substrate. *Eclética Química*, submitted.
- [70] Nassar E. J., Ciuffi K. J., Gonçalves R. R., Messaddeq Y., Ribeiro S. J. L. (2003). Filmes de titânio-silício preparados por “spin” e “dip-coating”, *Quim. Nova*, Vol. 26, pp. 674-678.
- [71] Bandeira L. C., de Campos B. M., de Faria E. H., Ciuffi K. J., Calefi P. S., Nassar E. J., Silva J. V. L., Oliveira M. F., Maia I. A. (2009). TG/DTG/DTA/DSC as a tool for studying deposition by the sol-gel process on materials obtained by rapid prototyping, *J. Thermal Analysis and Calorimetry*, Vol. 97, No. 1, pp. 67-70.
- [72] Peter M., Binudal N. S., Soumya S., Nair S.V., Furuike T., Tamura H., Kumar R. J. (2010). Nanocomposite scaffolds of bioactive glass ceramic nanoparticles disseminated chitosan matrix for tissue engineering applications, *Carbohydrate Polymers*, Vol. 79, pp. 284-289.
- [73] Bandeira, L. C., De Campos, B. M., Calefi, P. S., Ciuffi, K. J., Nassar, E. J., Silva, J. V. L., Oliveira, M. Maia, I. A. (2011). Coating On Organic Polymer With Macroporous Structure Prepared By Rapid Prototyping, *Journal of Nanostructured Polymers and Nanocomposites*, in press.
- [74] Rocha, L. A., Molina, E. F., Ciuffi, K. J., Calefi, P. S., Nassar, E. J. (2007). Eu (III) as a probe in titânia thin films: the effect of temperature, *Materials Chemistry and Physics*, Vol. 101, No. 1, pp. 238-241.
- [75] Rocha, L. A., Ciuffi, K. J., Sacco, H. C., Nassar, E. J. (2004). Influence on deposition speed and stirring type in the obtention of titânia films, *Materials Chemistry and Physics*, Vol. 85, No. 2-3, pp. 245-250.

- [76] Culbertson, B. M. (2001). Glass-ionomer dental restoratives. *Progress in Polymer Science*, Vol. 26, No. 4, pp. 577-604.
- [77] Nicholson, J. W. (1998). Chemistry of glass-ionomer cements: a review. *Biomaterials*, Vol. 19, No. 6, pp. 485-494.
- [78] Pires R., Nunes T. G., Abrahams I., Hawkes G. E., Morais C. M., Fernandez C. (2004). Stray-Field Imaging and Multinuclear Magnetic Resonance Spectroscopy Studies on the Setting of a Commercial Glass-Ionomer Cement. *J. Mater. Sci.: Mater. in Medicine*, Vol 15, pp. 201-208.
- [79] Wright J. D., Sommerdijk N. A. M. (2001). Sol-Gel Materials Chemistry and Applications. ISBN 90-5699-326-7 1a Edição, Gordon and Breach Science Publishers; Amsterdam, Holanda.
- [80] Yang Z., Lin Y. S. (2000). Sol-gel synthesis of silicalite/g-alumina granules. *Ind. Eng. Chem. Res.*, Vol. 39, pp. 944-948.
- [81] Stamboulis A., Hill R. G., Law R. V. (2004). Characterization of the structure of calcium alumino-silicate and calcium fluoro-alumino-silicate glasses by magic angle nuclear magnetic resonance (MAS-NMR). *J. Non-Cryst. Solids*, Vol 333, pp. 101-107.
- [82] Stamboulis A., Law R. V., Hill R. G. (2004). Characterisation of commercial ionomer glasses using magic angle nuclear magnetic resonance (MAS-NMR). *Biomaterials*, Vol. 25, pp. 3907-3913.
- [83] Pan J., Zhang H., Pan M. (2008). Self-assembly of Nafion molecules onto silica nanoparticles formed in situ through sol-gel process. *Journal of Colloid and Interface Science*, Vol. 326, pp. 55-60.
- [84] Cestari, A., Bandeira, L. C., Calefi, P. S., Nassar, E. J., Ciuffi, K. J. (2009). Preparation of calcium fluoroaluminosilicate glasses containing sodium and phosphorus by the nonhydrolytic sol-gel method *Journal of Alloys and Compounds*, Vol. 472, pp. 299-306.
- [85] Gorman, C. M., Hill, R. G. (2003). Heat-pressed ionomer glass-ceramics. Part I: an investigation of flow and microstructure *Dental Materials*, Vol. 19, No. 4, pp. 320-326.
- [86] Griffin, S. G., Hill, R. G. (1999), Influence of glass composition on the properties of glass polyalkenoate cements. Part I: influence of aluminium to silicon ratio. *Biomaterials*, Vol. 20, No. 17, pp. 1579-1586.
- [87] Phillips, R. W. (1993). Skinner Materiais Dentários, ISBN 85-7404-091-6. Editora Guanabara Koogan, 9a Edição, Rio de Janeiro, Brasil.
- [88] Brentegani L. G., Bombonato K. F., Carvalho T. L. (1997). Histological evaluation of the biocompatibility of a glass-ionomer cement in rat alveolus. *Biomaterials*, Vol 18, pp. 137-140.
- [89] Campos-Pinto M. M., de Oliveira D. A., Versiani M. A., Silva-Sousa Y. T., de Sousa-Neto M. D., da Cruz Perez D.E. (2008). Assessment of the biocompatibility of Epiphany root canal sealer in rat subcutaneous tissues. *Oral Surg Oral Med Oral Pathol Oral Radiol Endod*, Vol 105, pp. 77-81.,
- [90] Garcia, L. da F. R., de Souza, F. de C. P. P., Teófilo, J. M., Cestari, A., Calefi, P. S., Ciuffi, K. J., Nassar, E. J. (2010). Synthesis and biocompatibility of na experimental glass ionomer cement prepared by a non-hydrolytic sol-gel method, *Brazilian Dental Journal*, Vol. 21, No. 6, pp. 499-507.



## **Biomaterials Science and Engineering**

Edited by Prof. Rosario Pignatello

ISBN 978-953-307-609-6

Hard cover, 456 pages

**Publisher** InTech

**Published online** 15, September, 2011

**Published in print edition** September, 2011

These contribution books collect reviews and original articles from eminent experts working in the interdisciplinary arena of biomaterial development and use. From their direct and recent experience, the readers can achieve a wide vision on the new and ongoing potentials of different synthetic and engineered biomaterials. Contributions were not selected based on a direct market or clinical interest, than on results coming from very fundamental studies which have been mainly gathered for this book. This fact will also allow to gain a more general view of what and how the various biomaterials can do and work for, along with the methodologies necessary to design, develop and characterize them, without the restrictions necessarily imposed by industrial or profit concerns. The book collects 22 chapters related to recent researches on new materials, particularly dealing with their potential and different applications in biomedicine and clinics: from tissue engineering to polymeric scaffolds, from bone mimetic products to prostheses, up to strategies to manage their interaction with living cells.

### **How to reference**

In order to correctly reference this scholarly work, feel free to copy and paste the following:

Eduardo J. Nassar, Katia J. Ciuffi, Paulo S. Calefi, Lucas A. Rocha, Emerson H. De Faria, Marcio L. A. e Silva, Priscilla P. Luz, Lucimara C. Bandeira, Alexandre Cestari and Cristianine N. Fernandes (2011). Biomaterials and Sol–Gel Process: A Methodology for the Preparation of Functional Materials, Biomaterials Science and Engineering, Prof. Rosario Pignatello (Ed.), ISBN: 978-953-307-609-6, InTech, Available from: <http://www.intechopen.com/books/biomaterials-science-and-engineering/biomaterials-and-sol-gel-process-a-methodology-for-the-preparation-of-functional-materials>

**INTECH**  
open science | open minds

### **InTech Europe**

University Campus STeP Ri  
Slavka Krautzeka 83/A  
51000 Rijeka, Croatia  
Phone: +385 (51) 770 447  
Fax: +385 (51) 686 166  
[www.intechopen.com](http://www.intechopen.com)

### **InTech China**

Unit 405, Office Block, Hotel Equatorial Shanghai  
No.65, Yan An Road (West), Shanghai, 200040, China  
中国上海市延安西路65号上海国际贵都大饭店办公楼405单元  
Phone: +86-21-62489820  
Fax: +86-21-62489821

© 2011 The Author(s). Licensee IntechOpen. This chapter is distributed under the terms of the [Creative Commons Attribution-NonCommercial-ShareAlike-3.0 License](https://creativecommons.org/licenses/by-nc-sa/3.0/), which permits use, distribution and reproduction for non-commercial purposes, provided the original is properly cited and derivative works building on this content are distributed under the same license.

IntechOpen

IntechOpen